STUDIES ON METHYLENE BLUE DYE ADSORPTION, USING CARBONIZED, ACTIVATED CARBON AND MAGNETIC CARBONIZED SAMPLES FROM KENTUCKY COFFEE TREE PODS

A Thesis Presented to the Department of Materials Science and

Engineering

African University of Science and Technology

In Partial Fulfilment of the Requirements for the Degree of

Master of Science

by

Yakubu Nimota Adenike

Abuja, Nigeria

April 2021

CERTIFICATION

This is to certify that the thesis titled “Studies on Methylene Blue Dye Adsorption, Using Carbonized, Activated Carbon and Magnetic Carbonized Samples from Kentucky Coffee Tree Pods” submitted to the school of postgraduate studies, African University of Science and Technology (AUST), Abuja, Nigeria for the award of Master's degree, is a record of original research carried out by Yakubu Nimota Adenike in the Department of Materials Science and Engineering.

STUDIES ON METHYLENE BLUE DYE ADSORPTION, USING CARBONIZED, ACTIVATED CARBON AND MAGNETIC CARBONIZED SAMPLES FROM KENTUCKY COFFEE TREE PODS

by

Yakubu Nimota Adenike

A THESIS APPROVED BY THE MATERIALS SCIENCE AND ENGINEERING DEPARTMENT

RECOMMENDED: ----------

Supervisor, Professor A.P. Onwualu

Head, Department of Materials Science and Engineering

Professor A.P. Onwualu

APPROVED: ----------

Chief Academic Officer

Date

ABSTRACT

This study was carried out under various experimental conditions and rate of dye adsorption such as the solution pH, the adsorbent preparation concentration, and contact time to assess the potentiality of Kentucky coffee pods (KCP) for the removal of Methylene Blue (MB) dye from wastewater. From KCP, precursors were obtained by Carbonization at varying impregnation ratio, Magnetic Carbonization/Activation. Carbonization was performed at 500^0C, KOH used for chemical activation impregnation at ratio 1:1 and 1:4. The activated carbon samples were heated at 800^0C. The Magnetic Carbonized/activated Carbon samples were modified with 40 mL of ammonia at 60^0C at 350 rpm. The dye adsorbate was investigated with UV-Vis for 50 min. Moreover, the resultant samples were characterized using SEM, FT-IR and EDX elemental analysis. Carbonized (pH7 and pH10) and MAC1:4 (pH4, pH6, and pH8) precursor preparation had the best dye adsorbate compared to AC1:1 and AC1:4. This is greatly associated with the dye solution pH, adsorbent preparation conditions.

KEYWORDS: Carbonized, Activated carbon, Magnetic Carbonized/Activated Carbon, Methylene Blue, Kentucky coffee tree pods, water purification.

ACKNOWLEDGEMENT

Glory be to Allah God for the privilege and gift of life to have completed this Master's program. Thanks to my HOD and supervisor, Prof. A. P. Onwualu, for his incredible support, fatherly and towering support. I acknowledge the resident faculties, Dr. A. Vitalis and Dr. A. Bello, the Laboratory scientist, Mr. Tony. Dr. K. Moses and Miss Uchechukwu Ezealigo (Ph.D. student) for putting me through the research lab work. Thanks to my M.Sc. scholarship sponsors, the African University of Science and Technology (AUST). The donor of the laboratory where the studies were done, the African Development Bank (AfDB) and Pan African Materials Institute (PAMI); and others who contributed to my success.

DEDICATION

This thesis is dedicated to Almighty Allah, my husband Alhaji M.A. Alade, my parents Mr. and Mrs. Yakubu and my siblings for their loving support and encouragement.

TABLE OF CONTENTS

LIST OF FIGURE

CHAPTER TWO

CHAPTER THREE

CHAPTER FOUR

LIST OF TABLE

CHAPTER ONE
INTRODUCTION

1.1 Background

Industrial wastewater is considered one of the major pollutants of the environment (Derakhshan et al., 2013). Various industries such as mining, mineral extraction, plastic, textile, cosmetics, printing, food, pharmaceutical, chemical, petroleum, paper, nuclear, leather, paint, and automobile, as well as for the treatment of drinking water, industrial and urban wastewater (Safarik et al., 2012) produce colored wastewater that requires a continuous and effective water purification plan. Such colors not only change the water's color, which is important regarding aesthetics, but they also prevent light from penetrating through water, disturb photosynthesis, and destroy the aquatic ecosystem as well as several aquatic species (Derakhshan et al., 2013) when charged into streams, rivers or lakes. According to (Geçgel et al., 2013) "Discharge of these colored effluents presents a major environmental problem for developing countries because of their toxic and carcinogenic effects on living beings. Dyes often used in these industries, can be divided into acidic, reactive, direct, basic, and other groups (Samarghandi et al., 2012)

Many methods such as activated carbon sorption, chemical coagulation, ion exchange, electrolysis, and biological treatments have been developed for removing dye pollutant from wastewater before being discharged into the environment. Of these methods, activated carbon sortion is highly effective for the removal of dyes and pigments as well as other organic and inorganic pollution. Previous research efforts have shown that different biomass can be valorized into activated carbon that can be used for removing the dyes and hence contribute in water purification.

There is need to evaluate different methods of making activated carbon and also evaluate the effectiveness of activated carbon made from different biomass in removing the dyes and other pollutants from waste water. Kenturky coffee tree pods were chosen as the raw materials for making activated carbon in this study.

1.2 Objectives

The main aim of the study was to develop activated carbon from Kentucky coffee tree

pods and determine its capacity for water purification. The objectives of this research were to:

- develop activated carbon from Kenturky coffee tree pods;
- determine the effect of different pH on dye adsorbance;
- determine the effect of varying time on dye adsorbance;
- compare the different concentration of activated carbon charcoal:
- compare magnetic and non-magnetic carbonized adsorbance:
- compare carbonized, magnetic carbonized, activated carbon, and magnetic-activated carbon absorbance in the same dye environment with respect to time.

1.3 Statement of Purpose

This project work was executed to determine the most effective means of dye adsorbate and purification of methylene blue. The aim was to identify the best method of bio-charcoal preparation with respect to pH and contact time.

1.4 Scope of Work

In the course of contributing to industrial wastewater treatment and dye absorbance, bio charcoal also known as biochar, of different kinds of organic biomass have been used over time for dye absorbance. Biochar is a carbon-rich highly porous substance obtained after pyrolysis of organic biomass. The production of biochar is a sustainable option for waste and disease management. It contains more than 50% of the original carbon which is highly recalcitrant; therefore its production helps in carbon sequestration by locking the carbon present in the plant biomass. The elemental composition and structural configuration of biochar are strongly correlated with temperature, heating rate, activation atmosphere, and residence time maintained during its production (Rumi Narzari1, 2015). The Kentucky coffee tree (Gymnocladus dioicus, Fabaceae) is a rare, usually dioecious tree of eastern and mid-western North America. Its range in nature extends from southern Ontario in the north, west to Minnesota, south to Arkansas, and north and east to New York (Zaya & Howe, 2009), it is also found across the world. Over time, researchers report that the seeds and pods are poisonous. They reportedly contain cytisine, a quinolizidine alkaloid and nicotinic receptor agonist, which can be dangerous (Scott Peterson, 2021). Aside from using Kentucky coffeetree pods as an ornament, it can also find a new application in organic biomass to

be carbonized for dye absorbance as biochar is a known sustainable option for waste and disease management (Rumi Narzari1, 2015). Alternatively, some common names for the tree include American coffee berry, chicot, coffee-bean, Kentucky mahogany, nicker tree, and stump tree (Bjerregaard, 2008). The state tree of Kentucky should be used more often because it is adaptable to many soils, including alkaline (Gilman & Watson, 2021). It is assumed the large seed pods hang on the tree in the winter but can be a litter problem when they fall in the spring (Gilman & Watson, 2021). Although little is known about the specific uses of Kentucky coffeetree by early Native Americans of the Great Lakes region, through careful comparisons to similar species, a more thorough understanding of the ethnobotanical practices of its users, and through a better understanding of the tree itself, much can be construed (Vannatta, 2009). Over time, researchers report that the seeds and pods are poisonous. They reportedly contain cytisine, a quinolizidine alkaloid and nicotinic receptor agonist, which can be dangerous (Scott Peterson, 2021).

1.5 Justification for the Study

Over time, different kinds of organic biomass have been used for dye absorbance. Many dye removal processing methods have been tried to deal with this problem, but only the adsorption method is superior to other methods (Saputra et al., 2018). Therefore, much focus and progress have been given to the chemical modification of activated carbon. Mercury(II) is a soft acid and simple to form a stable complex with soft alkali, based on the theory of hard and soft acid-base (HSAB), and the reaction process between mercury(II) and soft alkali has a high complexation rate (Lou et al., 2012). However, there are no reports of obtaining activated carbon from Kentucky coffee tree pods by chemical and physical activation methods (Geçgel et al., 2013). Therefore, in this research, the adsorption equilibrium of methylene blue on activated carbon from Kentucky coffee tree pods was studied. The adsorption of MB using uniquely prepared samples ranging from raw KCP, carbonized, AC, and MAC was examined as a function of pH, temperature, initial dye concentration, adsorbent concentration, and contact time.

CHAPTER TWO
LITERATURE REVIEW

2.1 Carbonization

Carbonization is an aromatic growth and polymerization process in which the fiber is treated at high temperatures in an inert condition up to 800–3000°C to remove the noncarbon elements as volatile gases, such as nitrogen, hydrogen cyanide methane, hydrogen, carbon dioxide, water, carbon monoxide, ammonia, and other gases. The process takes place after stage stabilization, whereby stabilized precursor fibers are converted into high-strength Carbon Fiber spinning CFs (Zhang & Li, 2017). Carbonization under pressure is classified into three:

(1) Carbonization under pressure built-up by the decomposition gases of the precursor,
(2) carbonization under hydrothermal conditions and,
(3) reduction of CO_2 under pressure (Inagaki et al., 2014a).

During carbonization (high-temperature phase) in an inert atmosphere, usually nitrogen, the stabilized fibers are passed through zones of increasing temperature to around 1500 °C. This is the first stage in which the structure of the carbon fiber and associated properties are formed (Gupta & Afshari, 2009). Carbonization is aimed at controlling the morphology and pore structure of carbon materials. Carbon materials in tubular, lamellar, and foam morphology are synthesized by using inorganic layered compounds, anodic aluminum oxide films, and organic foams respectively (Inagaki et al., 2014b). Carbonization materials are made from almost all organic materials containing carbon, such as wood, sawdust, nutshells, fruit stones, peat, lignite, coal, coke. The use of an appropriate precursor depends primarily on its availability and cost, while it also depends on the main applications of the carbon produced and the type of installation available (Marsh & Rodríguez-Reinoso, 2006). The process of carbaonization is illustrated in Fig. 2.1.

2.1.1 Optimum Utilization of Biomass wastes for Carbonization

Researchers over time have come up with different kinds of organic biomass waste with different methods of preliminary sample preparation, starting with the washing of the biomass and cutting into a smaller bit.

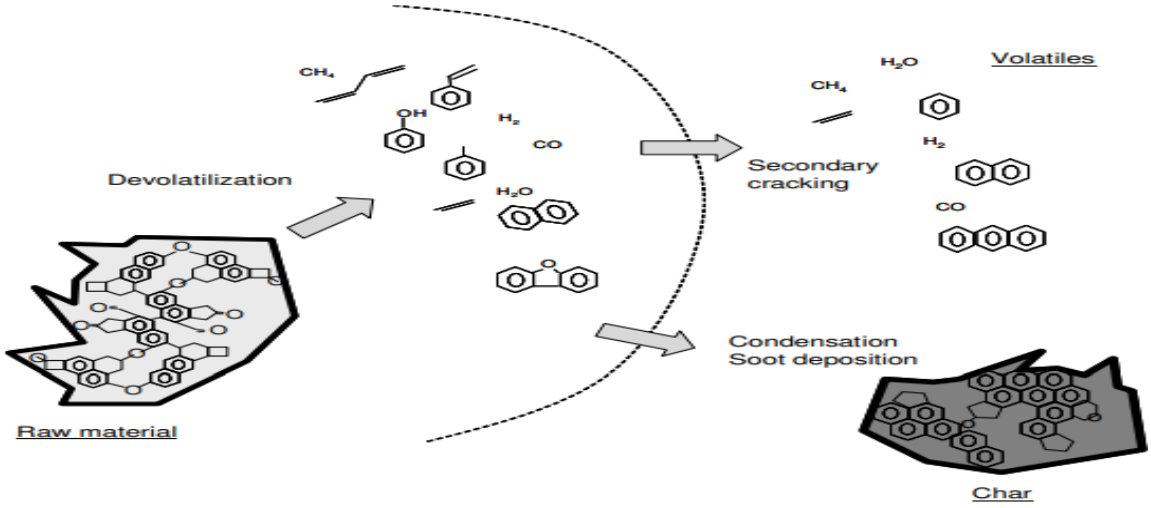

Figure 2.1: Typical method of carbonization response of a carbonaceous material (Menéndez-Díaza & Martín-Gullónb, 2006)

Plantain stems have been uswd for making activated carbon (Ekpete et al., 2017a). Plantain stems cut into smaller bits and sundried for 3-4 days, then oven-dried for 8 hours at a temperature of 120^0C and pulverized into a fine powder. Carbonization was performed at a temperature of 400^0C for 1 hr using the box-type resistance furnace. Also, (Cazetta et al., 2016) utilized coconut shells, these were put in a muffle furnace and heated at a rate of 20°C min^{-1} from room temperature to 700°C, held for 1.5 hr at 700°C under a flow of N_2 at a rate of 100 cm^3 min^{-1}. The produced biochar was allowed to cool down overnight in the furnace (Vithanage et al., 2016). Biochar (BC) is produced at 700^0C pyrolysis temperature since previous studies have proved that high temperature derived BCs are greatly effective in the remediation of organic and inorganic pollutants (M. Ahmad et al., 2012).

As documented by (LIM, 1996), at terminal temperatures of 400-550°C with holding times of 1-3 h and two heating speeds, carbonization of oil palm trunks to produce charcoal was performed. The result shows that the quantity and quality of the charcoal produced are not affected by the holding period, while the heating rate has a minor effect. However, as the terminal temperature rises, while the fixed carbon content

increases, both yield, and volatile content decrease. The calorific value and the ash content are independent of the studied parameters and 4032 kcal/kg and 37.2 percent are their respective values. As the calorific value is low and the ash content is high, it is concluded that for the production of charcoal fuel, oil palm trunks are not suitable. In another research, two samples were used as a precursor: carbon-based coal obtained by carbonization and a raw carbon oxidized gas-phase sample. The adsorption parameters and diffusion coefficients of the NO-carbon catalyst system were obtained using the TAP-2 (Temporary Study of Products) reactor. After increasing the number of functional groups by oxidative pretreatment of carbon, the diffusivity of both NO and adsorption enthalpy does not alter (Fierro et al., 2002).

2.2 Activation of Carbonization Process

Activated carbon (AC), generally for small molecules, has a large adsorption potential and is used for liquid and gas purification. A variety of activated carbon with distinct porosities can be obtained by monitoring the carbonization and activation phase. AC is commonly used in granular and powdered forms, but it can also be produced by controlled carbonization in textile form. To improve its adsorptive properties, AC is porous carbon fiber, a char that has been subjected to reaction with gases, often with the addition of chemicals such as $ZnCl_2$ before, during, or after carbonization (Marsh & Rodríguez-Reinoso, 2006). AC exhibits amphoteric properties and is generally used for organic and inorganic compound adsorption (Tehrani-Bagha & Balchi, 2018). By intensifying impregnation of various forms of AC in iron salt solution, accompanied by drying and heat treatment at 200 °C, AC assisted catalysts can be easily prepared (Tehrani-Bagha & Balchi, 2018) using phenol as the target pollutant, a highly stable $Fe/\gamma\text{-}Al_2O_3$ catalyst for catalytic wet peroxide oxidation has been studied. The catalyst was prepared with an aqueous solution of $Fe(NO_3)_3{\cdot}9H_2O$ via the incipient wetness impregnation of $\gamma\text{-}Al_2O_3$ (Bautista et al., 2011).

As an active stage, transition metals, principally iron and copper, are used as catalyst stage, for the elimination of organic compounds. Several materials, containing mainly iron and copper precursors backed by oxides are proposed. The benefits of a heterogeneously catalyzed mechanism are demonstrated by the catalysts. They have

comparatively greater oxidation efficiency and lower sensitivity of pH under similar conditions, unlike a homogeneous catalyst (Valkaj et al., 2011).

For the preparation of activated carbon, two methods can be used in water purification processes: physical activation and chemical activation (Asif Ahmad & Azam, 2019). Due to its greater surface area, microporous strength, and chemical complexity of its exterior area, activated carbon has a strong potential to adsorb heavy metals. Two forms of stimulated active carbon are available: H-type and L-type (Zelmanov & Semiat, 2014). When introduced into water or treated with strong acids, the H-type carbon adopts positive charges and is characterized as hydrophobic. The L-type carbon is a stronger solid acid than the H-type carbon which assumes a negative charge in water which neutralizes strong bases and is hydrophilic. Based on its physical appearance, activated carbon is divided into four basic groups. Powders (PAC), fibrous (ACF), granular (GAC), and clothe (ACC). Commercial activated carbon (CAC) is used more widely worldwide (Mudakavi & Puttanna, 2016).

2.2.1 Factors Involved in the optimization of AC

The characteristics and yield of activated carbon are determined by the types of biomass and the activation conditions. Researchers such as (Rajamani et al., 2018) evaluated activated carbon made from sterculia foetida as an adsorbent using phosphoric acid as activating agent. The optimum condition for activation is found to be the impregnation ratio of 1:5, Activation Temperature of 700 ^{o}C, and Activation Time of 90 min. When the impregnation ratio increases, the more swelling of the material and hence stronger release of volatiles leading to increased pores. Methylene blue number of mg g^{-1} indicates that the prepared activated carbon is more in micropores and less in mesopores. It is found that coir with very low bulk density and the porous structure is a valuable raw material for the production of highly porous activated carbon and other essential factors such as its high carbon content. In an inert nitrogen atmosphere, both carbonization and activation were done in one step to increase the surface area and establish interconnecting porosity. Compared to that produced by physical activation (1365 m2/gm), activated carbon provided by a combination of chemical and physical activation has a higher surface area of 2442 m2/gm (Manocha et al., 2013). A review by (Heidarinejad et al., 2020) compared the method of physical mixing and the method of impregnation with alkali metals inactivation, also reveals that the activated carbon obtained by physical mixing had a higher

porosity than the activated carbon provided by the method of impregnation. However, (Derakhshan et al., 2013) in their results showed that with increasing initial dye concentration, pH, and contact time, the adsorption of the Methylene Blue was enhanced. The optimum pH was 10. The Langmuir model's q_{max} for adsorption of methylene blue dye was 15.87 mg/g. The Freundlich isothermal model and pseudo-second-order kinetic model had the best fitness, given the R^2 (0.999) and χ^2 values.

2.3 Magnetic Activated Carbon

For environmental remediation and human protection, the production of advanced carbon nanomaterials that can efficiently remove contaminants from solutions is of great importance. This is achived via simultaneous activation and magnetization processes using carbonized biomass waste and $FeCl_3 \cdot 6H_2O$ as precursors (Cazetta et al., 2016). The key point of the synthetic strategy is that the carbonization, activation, and Fe_3O_4 loading are accomplished simultaneously, via thermic activation/magnetization. Magnetically activated carbon preparation is primarily concentrated on a two-step process based on the finished activated carbon. The magnetic material (or precursor) is mixed with the activated carbon in a "physical-mechanical" process with bonding, milling, adsorption, chemical co-precipitation, or secondary activation to obtain carbon/magnetic composite materials. The adsorption technique, the chemical coprecipitation technique, is the most documented among them. The method of adsorption is based on how the magnetic fluid is prepared. In the solution containing the magnetic fluid, the activated carbon is immersed and constantly stirred and the excess magnetic fluid is collected by pickling or ultrasonic removal, Magnetic activated carbon is thus, obtained.

At present, Fe3O4 and γ-Fe_2O_3 are primarily recorded in the magnetic fluids used in the adsorption process (Luo & Zhang, 2009). Coprecipitation is primarily used for the preparation of the magnetic fluid Fe_3O_4. The measures are shown as follows: salts of Fe (III) and Fe (II) are prepared with a certain proportion into a solution. And ammonia is added as a precipitant, or sodium hydroxide. The chemical co-precipitation process involves first immersing the finished activated carbon in a mixed solution of Fe (III) and Fe (II) salt to penetrate or adsorb Fe^{2+} and Fe^{3+} in the activated carbon pores and then adjusting the pH to obtain iron hydroxide. Increase the temperature to turn the iron

hydroxide into iron oxide. Magnetic activated carbon is thus obtained from magnetic particles. However, both methods add magnetic particles to the finished activated carbon, so the pores of the activated magnetic carbon are easily blocked as well (Zheng, 2020).

Magnetic carbon activated (MAC) Fe_3O_4-loaded activated carbon was established using termite excrement and sulfuric acid as the carbon-modifying agent (Demarchi et al., 2019). Magnetically modified multi-wall carbon nanotubes (M-MWCNT) and activated carbon (M-AC) were prepared as precursors by the chemical co-precipitation process with Fe^{2+}:Fe^{3+} salts (Bayazit & Kerkez, 2014) and the carboxylic acid vapor treatment technique (Han et al., 2013). With the addition of the magnetic activated carbon, the color of the solution significantly faded. Subsequently, fast aggregation of the magnetic activated carbon from their homogeneous dispersion in the presence of an external magnetic field could be seen (Gao et al., 2016). It is considered a major challenge to maintain the stability of Fe nanoparticles, as Fe nanoparticles are rapidly oxidized in water and air, resulting in magnetism and dispersibility loss or reduction. Overcoming this pattern (Haham et al., 2015) controlled co-precipitation technique was used to prevent undesirable critical oxidation of Fe^{2+} and Fe^{3+} (Kim et al., 2001).

2.4 Methylene Blue

One of the high-consuming materials in the dye industry is Methylene Blue (MB) which is used for cotton and silk painting (Robinson et al., 2001). The molecular stcurture of MB is shown in Fig.2.2. According to (Jayajothi et al., 2017), MB adsorption onto solids and its recognized usefulness in characterizing adsorptive material. MB is employed to evaluate the adsorption characteristics of carbon. Several methods have been proposed to remove dyes from the industrial wastewater among which adsorption is the most acceptable due to its cost-effectiveness and its capability to be used on large scales

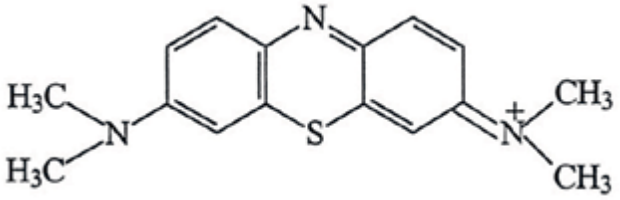

Figure 2.2: Molecular Structure of Methylene Blue (Derakhshan et al., 2013)

There is a need to find alternative treatments that are effective in removing dyes from large volumes of effluents and are low in cost, such as biological or combination systems (Robinson et al., 2001).

2.4.1 Ultraviolet-visible spectroscopy (UV-vis) Methylene blue peak

Ultraviolet-visible spectroscopy (UV-vis) is a type of absorption in which a molecule absorbs UV-visible light. UV-visible radiation absorption results in the excitation of electrons from lower to higher energy levels. Inorganic molecules, only certain functional groups (chromophores) containing low-excitation valence electrons can absorb ultraviolet and visible radiation (Pentassuglia et al., 2018). UV-vis spectroscopy is commonly used to quantitatively evaluate elemental concentrations in a solution according to the Beer-Lambert law:

$$\boldsymbol{A = Log_{10}\,(I_o/I) = \varepsilon cL,}$$

Where *A* is the measured absorbance, $\boldsymbol{I_o}$ is the intensity of the incident light at a given wavelength, $\boldsymbol{I}$ is the transmitted intensity, $\boldsymbol{\varepsilon}$ is a constant known as the molar absorptivity or extinction coefficient for each species and wavelength, $\boldsymbol{c}$ is the concentration of the absorbing species, and $\boldsymbol{L}$ is the path length through the sample. In quantitative analysis, $\boldsymbol{\varepsilon}$ at the wavelength of maximal absorption (λ_{max}) is typically used as errors arising from instrumental wavelength, variability is reduced at the height of the absorbance curve. According to this correlation, when $\boldsymbol{\varepsilon}$ is known, $\boldsymbol{L}$ is set, and $\boldsymbol{I_0}$ and $\boldsymbol{I}$ are measured, the analyte concentration can be determined. When an analyte calibration curve is available, the analyte concentration can be measured more precisely (Wang & Chu, 2013).

An attempt was made to study the adsorption of dyestuff Methylene Blue by α-chitin nanoparticles (CNP) prepared from *Penaeus monodon* shell waste. The study used unique nanoparticles of ⩽50 nm for the dye adsorption process (Dhananasekaran et al., 2016). The aqueous solution of methylene blue absorbs light at around 664 nm and displays brilliant blue. As is well known, the characteristic absorption peak of methylene blue about 664 nm decreases smoothly with a slight change towards a shorter wavelength when the aqueous solution is subjected to photocatalytic redox

reactions sensitized by TiO_2, and the solution gradually becomes colorless (Takahisa Omata, 2003).

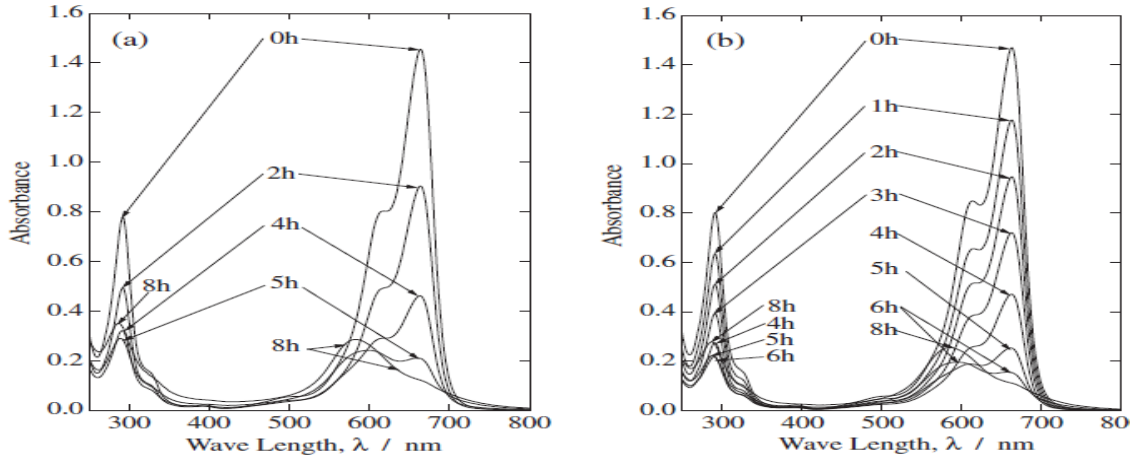

Figure 2.3: Variation in the absorption spectrum of methylene blue aqueous solution, sensitized by k-$CeZrO_4$ powder, under irradiation with 500 W Xe discharge light. The concentration of methylene blue in the starting solution of 2 x 10^{-5} mold-m^{-3}. (a): unfiltered irradiation, (b): irradiation with > 420 nm using L42 filter (Takahisa Omata, 2003).

2.5 Physical Properties of Activated Carbons

The porous carbon structure of carbon adsorbents requires small quantities of various heteroatoms, such as oxygen and hydrogen. Some activated carbons, depending on the quality of the raw material used as a precursor, often contain variable quantities of mineral matter (ash content). Perhaps the primary physical property that characterizes activated coal is the porous structure. This is formed by pores of different sizes which according to IUPAC recommendations (Siemieniewska, 1985) can be classified into three major groups

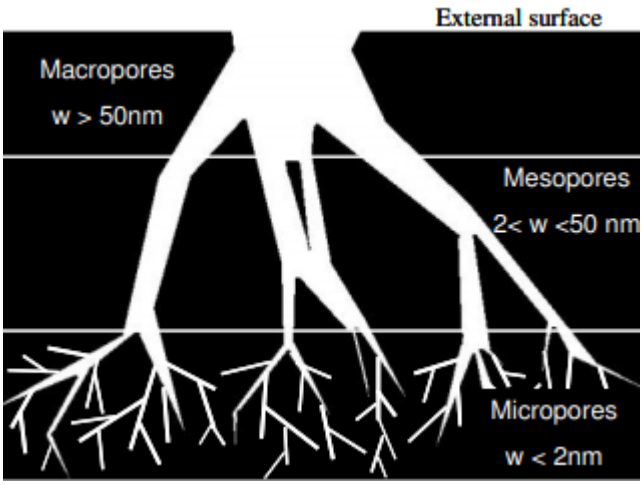

Figure 2.4: Schematic representation of a carbon adsorbent's pore network (Menéndez-Díaza & Martín-Gullónb, 2006)

- Micropores with a pore width of less than $2 \cdot 10^{-9}$ m.
- Mesopores with widths from 2.0 to $50 \cdot 10^{-9}$ m.
- Macropores with a pore width larger than $50 \cdot 10^{-9}$ m.

2.6 Surface Chemistry of Carbon

It has already been pointed out that for a carbon adsorbent to perform well in a specific application, a high surface area and an acceptable pore size distribution are required conditions. There are several examples of carbons with similar textural properties, however, which display a somewhat different capacity of adsorption with the same adsorbate (Biniak et al., 2017) it is also important to take into account the existence and quantity of the surface groups that may be present on carbon surfaces. The activated carbons' surface chemistry influences theirs: Catalytic properties, Moisture content, Character of acid-base, Ability of adsorption (Aznar, 2011). Three factors are specifically attributed to these heteroatoms contained on the activated carbon surface: the starting content, the process of activation, and the conditions of the treatment; and they are chemically bonded to the carbon surface during carbonization and activation, forming structures of carbon heteroatoms (Considine et al., 2001). In addition to reacting with oxygen, oxygen-containing surface groups can also result from reactions with many other oxidizing gases such as ozone, nitrous oxide, carbon dioxide, etc., and with oxidizing solutions such as nitric acid, hydrogen peroxide.

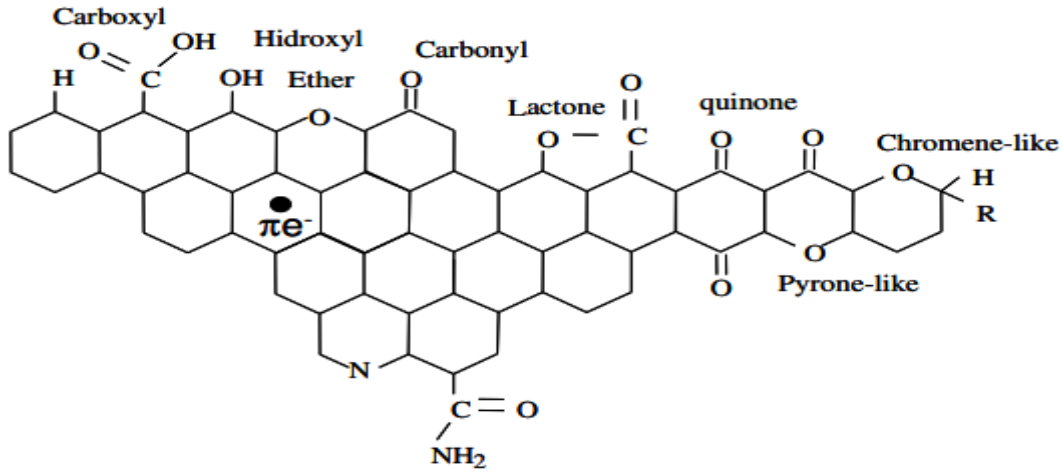

Figure 2.5: The most significant surface group forms that can be found on a carbon surface (Menéndez-Díaza & Martín-Gullónb, 2006)

Activated carbon surface chemistry can therefore be customized by oxidation with different agents to establish oxygen functionality or by heat treatment to eliminate them either selectively or entirely, depending on the temperature used. The most important kinds of surface groups that may be present on carbon surfaces are summarized in the Figure below. The most important kinds of surface groups that may be present on carbon surfaces are summarized in Figure 2.5.

CHAPTER THREE
MATERIAL AND METHODOLOGY

3.1 Materials and Equipment

3.1.1 Materials

Kentucky coffee tree pods (KCP), crucibles of different sizes, beakers of ranging sizes, Distilled water, De-ionized water, Nitrogen gas, Methylene blue dye, Ziplock airtight bags, paper tape, KBr Salt, Fe (III), and Fe (II) salts

3.1.2 Equipment

Carbolite Modular Horizontal Tube Furnace, Muffle Furnace, Orbital shaker, Eppendor Centrifuge 5804 R, Desiccator, Measuring cylinder, Drying Oven, 3 necked round bottom flask, Magnetic stirrer, Magnetic cooker, UV-Vis Specord 200 plus, OHAUS electrical lab balance, Thin-Film Compressor, Grinding Blender, 1.0 mm Sieve, and Measuring Scale.

3.2 Methodology

3.2.1 Sample Collection and Preparation

Kentucky coffee tree pods (KCP) were acquired from farmlands within the African University of Science and Technology (AUST) Abuja, Nigeria. The pods were deseeded, split into smaller pieces, thoroughly washed with de-ionized water, and sundried for 48 hrs. The dried samples were ground with a blender and sieved to fraction using a 1.0 mm sieve. The sieved sample was stored in a clean zip lock airtight bag.

3.2.2 Carbonization Operation

The carbonization process was done using the Carbolite Modular Horizontal Tube Furnace. The furnace was loaded with 200 g of the dried precursor into the furnace, and heated up to a carbonization temperature of 500°C, at 10 ^{o}C ramps/min for 1 hr (Geçgel et al., 2013) under purified nitrogen gas flow (150 cm^3/min) (Foo & Hameed, 2012) to create an inert atmosphere with holding times of 1 hr (LIM, 1996), The sample was allowed to cool to room temperature before collecting from the carbonizing furnace. Figure 3.1 below shows diagrammatically, the operations involved in achieving carbonization process:

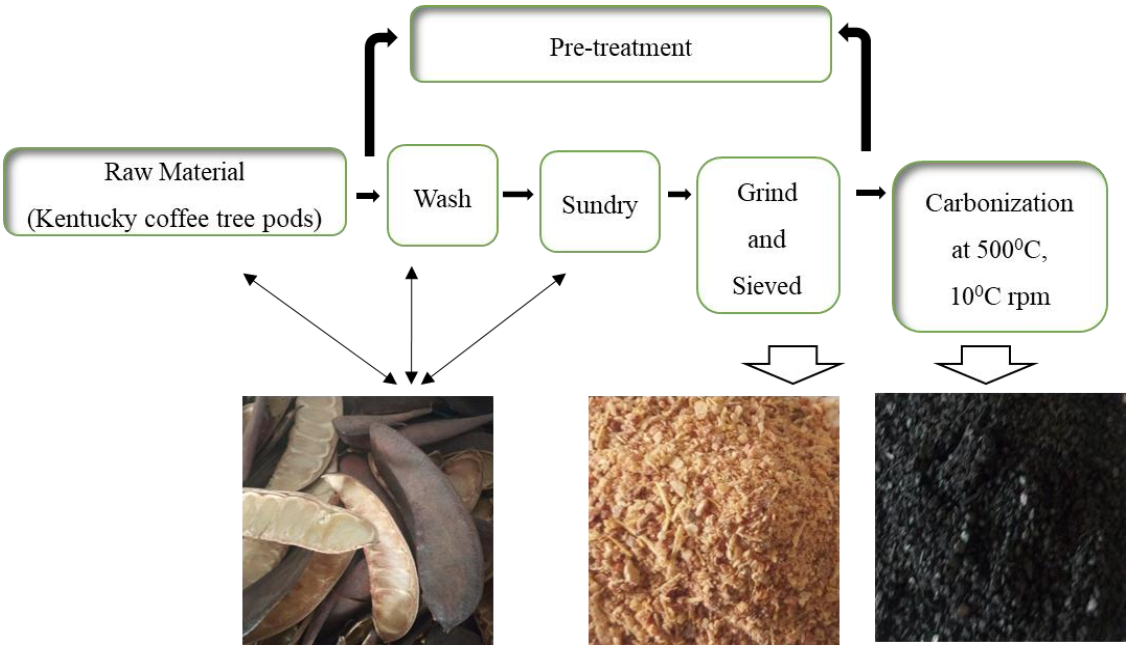

Figure 3.1: Kentucky coffee tree pods Carbonization flowsheet

3.2.3 Chemical Activation and Incubation of Carbonized sample

The charcoal product was allowed to cool (Ekpete et al., 2017a). 10 g of biochar was weighed out from the carbonized sample and then divided into two parts, sample A (5 g) and sample B (5 g). The chemical activation method was adopted to develop the pore structures and surface area (Danyuo et al., 2014). Potassium oxide (KOH) in two different masses (Fazal-Ur-Rehman, 2019) of 5 g and 20 g were poured into two separate beakers labeled A and B containing 50 mL of DW each as shown in Table 3.1.

The single-stage activation carbon synthesis was realized as follows (Zubrik et al., 2017): a fixed mass (5g) of the carbonized sample (A and B) was mixed with a different mass (5 g and 20 g) of KOH in 50 mL of distilled water (DW) each time to obtain 1: 1 and 1: 4, C: KOH ratios. A magnetic stirrer was then used to stir the mixture at 80°C, 700 rpm for 1 hr of incubation as seen in Figure 3.2. The obtained homogeneous mixture was put in an oven to dry at 105°C before being put into the Carbolite Modular Horizontal Tube Furnace to be activated at 800°C for 1 h under inert condition. Both carbonization and activation were performed at a heating rate of 10°C/min. Activation was accompanied by washing with 50 ml of dilute HCl and DW

till neutral pH was achieved; then samples were dried for 12 h using an oven at 100 °C. After drying, samples were stored in an airtight ziplock bag (Juma et al., 2020).

Table 3.1: Incubation sample preparation

Stage (ratio)	Beaker	Beaker Weight (g)	KOH (g)	CS (g)	DW(mL)
Stage-one (1:1)	A	169.8390	5	5.0	50
Stage-two (1:4)	B	169.9095	20	5.0	50

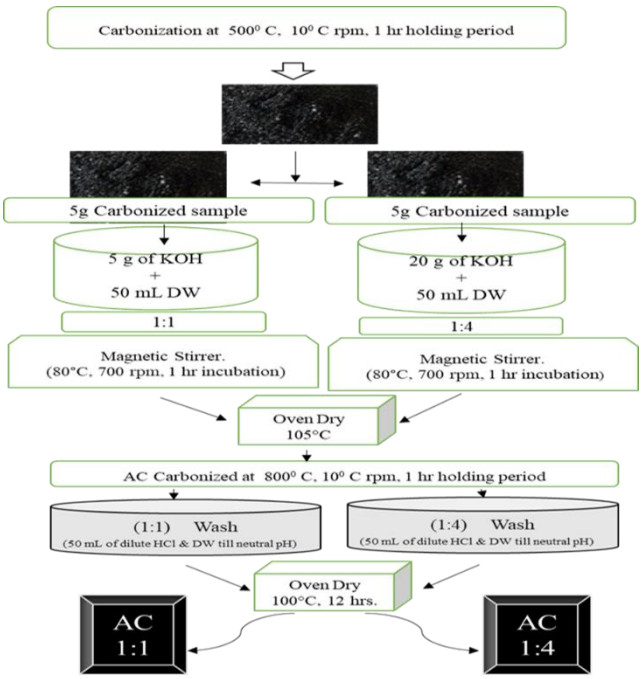

(a)

(b)

Figure 3.2: (a) Activation of Carbonization sample flowsheet. (b) A magnetic stirring of AC

3.2.4 Magnetic Activation of Carbonized samples

The adsorption method was based on the preparation of the magnetic fluid. The magnetic fluids used in the adsorption method Fe_3O_4 and γ-Fe_2O_3 are mainly reported by (Luo & Zhang, 2009). The steps involved were as follows:

- The mass of 4.8 g of Fe (III) and 3.0 g of Fe (II) salts was prepared into a solution (50 mL DW) in a 3 neck round bottom flask**;**
- 5.0 g of precursor (sample) was immersed in the solution containing the magnetic fluid (Zheng, 2020);

- The 3 neck round bottom flask containing the entire solution was placed on a thermal-magnetic stirrer to continuously stir the solution;
- The temperature was kept at 60^0C and 350 rpm;
- 40 mL of ammonia was added as a precipitant at the interval and purified Nitrogen gas was also passed through the solution at an interval to eliminate oxygen;
- Thus, the operation lasted for 30min;
- The MAC solution was washed with DW till a neutral pH was achieved;
- The washed MAC was dried in the oven at 100^0C for 5 hr.

The Magnetic operation was performed on MAC1:1, MAC1:4, and MC. Figure 3.3 shows the setup of magnetic activation carbon adopted:

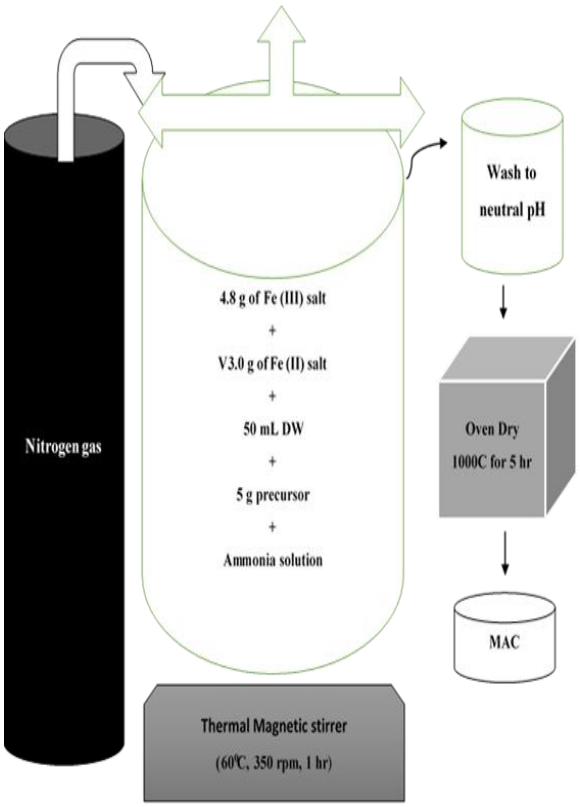

(a)

(b)

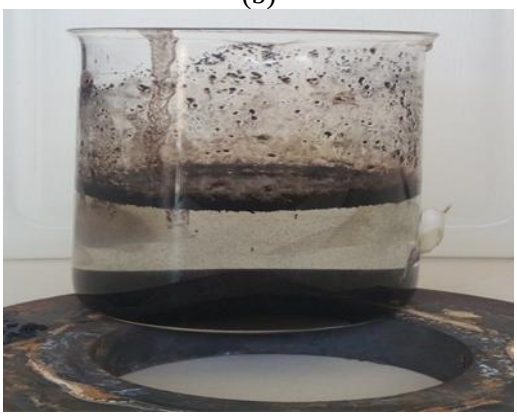

(c)

Figure. 3.3: (a) MAC flowsheet. (b) MAC set-up (c) Washing of MAC in DW with the aid of a magnetic metal block basement till neutral pH was achieved

3.3 Dye Solution Preparation

MB was employed to evaluate the adsorption characteristics in this research. Stepwise:

0.0020 g of MB was homogeneously dissolved in 2000 mL of Distilled Water (DW) to make a stock solution (SS); to serve as the overall reference, 5 mL solution was taped from the overall MB stock sample for UV-Vis analysis (Manufacturer: AnalytikJena Model: Specord 200 plus); 300 mL in five places was taped from the MB DSS; HCl and KOH in microdroplet were used to condition each 300 mL 0f the MB stock solution into the respective pH of 4, 6, 7, 8 and 10 (Getachew et al., 2015). Again, 5 mL solution was taped from each Conditioned Stock Solution (CSS) 300 mL pH stock sample for UV-Vis analysis to serve as the reference of each pH as shown in Figure 3.4:

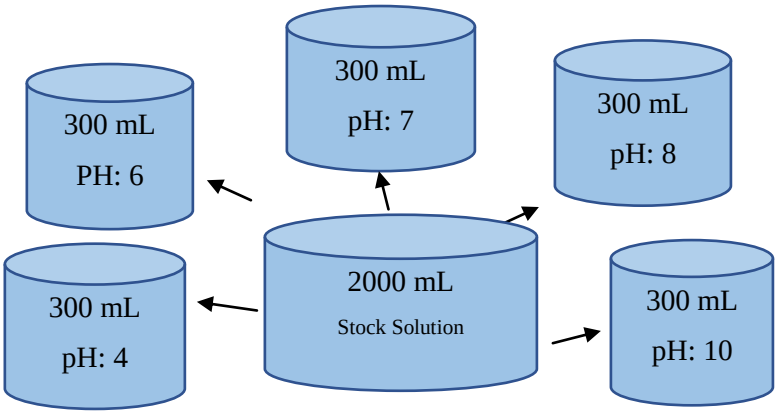

Figure 3.4: Conditioned stock solution into the respective pH of 4, 6, 7, 8 and 10

3.4 Adsorption Experimentation

This research focused on all possible ways of getting the best mode of adsorbate from single biomass. The following six precursors were coined out of Kentucky coffee tree pods:

1. Carbonized (CKCP);
2. Activated Carbon (AC1:1);
3. Activated Carbon (AC1:4);
4. Magnetic Carbonized (MC),
5. Magnetic Activated Carbon (MAC1:1);
6. Magnetic Activated Carbon (MAC1:4).

3.4.1 Batch adsorption experiments of Precursors

In a sequential order:

- 50 mL from each 300 mL already conditioned stock solutions of pH 4, 6, 7, 8,

10 was withdrew into a 200 mL beaker;

- Each beaker was labeled pH4, pH6, pH7, pH8, and pH10 respectively;
- The mass of 0.003 g MAC 1:1 precursor was added into each beaker;
- The beakers were relabeled (MAC1:1 pH4, MAC1:1 pH6, MAC1:1 pH7, MAC1:1 pH8, and MAC1:1 pH10) for easy identification;
- The beakers were place in different slot in the orbital shaker; as shown in Figure. 3.5;

(a) (b)

Figure 3.5: (a) Front view of the Orbital shaker. (b) Top view of the orbital shaker

- After every 10 min, 5 mL solution from each beaker are taped with the aid of a micropipette into a centrifuge tube for 50 min;
- The taped samples were centrifuge at 3000 rpm for 3 min at room temperature to separate the carbon particles from the solution;
- The adsorption capacity of carbonized char in the solution was then analyzed using UV-Vis. The experiment was analyzed on 6 different precursors as indicated in Table 3.2, except for R KCP which the pH was not varied:

Table 3.2: Adsorption capacity of six different precursors run on UV-Vis

Precursors**:** **CKCP, AC1:1, AC1:4, MC, MAC1:1, MAC1:4**				
pH4 10 min	pH6 10 min	pH7 10 min	pH8 10 min	pH10 10 min
pH4 20 min	pH6 20 min	pH7 20 min	pH8 20 min	pH10 20 min
pH4 30 min	pH6 30 min	pH7 30 min	pH8 30 min	pH10 30 min
pH4 40 min	pH6 40 min	pH7 40 min	pH8 40 min	pH10 40 min
pH4 50 min	pH6 50 min	pH7 50 min	pH8 50 min	pH10 50 min

The data generated from UV-Vis was estimated using the Beer-Lambert law:

$$\boldsymbol{A = \varepsilon C L},$$

$$\boldsymbol{C = \frac{A}{\varepsilon L}},$$

Where: $\boldsymbol{A}$ is the measured absorbance generated from UV-Vis, $\boldsymbol{\varepsilon = 95000\ L\ Mol^{-1} Cm^{-1}}$ Constant known as the molar absorptivity or extinction coefficient for each species and wavelength for methylene blue dye, $\boldsymbol{C}$ is the concentration of the absorbing species, and $\boldsymbol{L = 1\ Cm}$ path length through the sample (Wang & Chu, 2013). Methylene Blue Molar mass is a constant value at 319 g and concentration in g/L was achieved by the molarity:

$$Concentration, C\ (Mol/L) \times\ Molar\ Mass, M\ (g/Mol) = Molarity, m\ (g/L)$$

Removal efficiency (RE) (Juma et al., 2020) of the dye adsorption was calculated using the equation:

$$Removal\ efficienvy = \frac{Initial\ dye\ Concentration - Final\ dye\ Concentration}{Initial\ dye\ Cocentration} \times 100\%$$

Table 3. 3: UV-Vis data for pH4 CSS with six different char precursors

pH4					
Precursors	Time (min)	Absorbance	Concentration (Mol/L)	Concentration (g/L) left in solution	Concentration (g/L) Adsorbed
C	10	0.3995	4.20526E-06	0.00135	0.00165
	20	0.3799	3.99895E-06	0.00128	0.00172
	30	0.3778	3.97684E-06	0.00127	0.00173
	40	0.3696	3.89053E-06	0.00124	0.00176
	50	0.3419	3.59895E-06	0.00115	0.00185
AC1:1	10	0.8446	8.89053E-06	0.00284	0.00016
	20	0.7786	8.19579E-06	0.00262	0.00038
	30	0.7371	7.75895E-06	0.00248	0.00052
	40	0.6751	7.10632E-06	0.00227	0.00073
	50	0.6451	6.79053E-06	0.00217	0.00083
AC1:4	10	0.5134	5.40421E-06	0.00173	0.00127
	20	0.5150	5.42105E-06	0.00173	0.00127
	30	0.5215	5.48947E-06	0.00176	0.00124
	40	0.5225	0.0000055	0.00176	0.00124
	50	0.5337	5.61789E-06	0.00180	0.00120
MC	10	0.7484	7.87789E-06	0.00252	0.00048
	20	0.7055	7.42632E-06	0.00238	0.00062
	30	0.6989	7.35684E-06	0.00235	0.00065
	40	0.6964	7.33053E-06	0.00234	0.00066
	50	0.6775	7.13158E-06	0.00228	0.00072

MAC 1:1	10	0.3907	4.11263E-06	0.00132	0.00168
	20	0.3691	3.88526E-06	0.00124	0.00176
	30	0.3551	3.73789E-06	0.00120	0.00180
	40	0.3518	3.70316E-06	0.00118	0.00182
	50	0.3509	3.69368E-06	0.00118	0.00182
MAC 1:4	10	0.0824	8.67368E-07	0.00028	0.00272
	20	0.0321	3.37895E-07	0.00011	0.00289
	30	0.0990	1.04211E-06	0.00033	0.00267
	40	0.0820	8.63158E-07	0.00028	0.00272
	50	-0.0196	-2.06316E-07	-0.00007	0.00307

Table 3. 4: UV-Vis data for pH6 CSS with six different char precursors

pH6					
Precursors	Time (min)	Absorbance	Concentration (Mol/L)	Concentration (g/L) left in solution	Concentration (g/L) Adsorbed
C	10	0.2396	2.52211E-06	0.00081	0.00219
	20	0.2304	2.42526E-06	0.00078	0.00222
	30	0.2125	2.23684E-06	0.00072	0.00228
	40	0.2080	2.18947E-06	0.00070	0.00230
	50	0.1677	1.76526E-06	0.00056	0.00244
AC1:1	10	0.5673	5.97158E-06	0.00191	0.00109
	20	0.5433	5.71895E-06	0.00183	0.00117
	30	0.5313	5.59263E-06	0.00179	0.00121
	40	0.5282	0.00000556	0.00178	0.00122
	50	0.5265	5.54211E-06	0.00177	0.00123
AC1:4	10	0.5077	5.34421E-06	0.00171	0.00129
	20	0.5078	5.34526E-06	0.00171	0.00129
	30	0.5086	5.35368E-06	0.00171	0.00129
	40	0.5107	5.37579E-06	0.00172	0.00128
	50	0.5113	5.38211E-06	0.00172	0.00128
MC	10	0.6417	6.75474E-06	0.00216	0.00084
	20	0.6405	6.74211E-06	0.00216	0.00084
	30	0.6403	0.00000674	0.00216	0.00084
	40	0.6379	6.71474E-06	0.00215	0.00085
	50	0.6165	6.48947E-06	0.00208	0.00092
MAC 1:1	10	0.4649	4.89368E-06	0.00157	0.00143
	20	0.4180	0.0000044	0.00141	0.00159
	30	0.3657	3.84947E-06	0.00123	0.00177
	40	0.2708	2.85053E-06	0.00091	0.00209
	50	0.2291	2.41158E-06	0.00077	0.00223
MAC 1:4	10	0.3656	3.84842E-06	0.00123	0.00177
	20	0.3445	3.62632E-06	0.00116	0.00184
	30	0.2930	3.08421E-06	0.00099	0.00201
	40	0.2279	2.39895E-06	0.00077	0.00223

	50	0.1523	1.60316E-06	0.00051	0.00249

Table 3.5: UV-Vis data for pH7 CSS with six different char precursors

pH7					
Precursors	Time (min)	Absorbance	Concentration (Mol/L)	Concentration (g/L) left in solution	Concentration (g/L) Adsorbed
C	10	0.1667	1.75474E-06	0.00056	0.00244
	20	0.1079	1.13579E-06	0.00036	0.00264
	30	0.0895	9.42105E-07	0.00030	0.00270
	40	0.0846	8.90526E-07	0.00028	0.00272
	50	0.0834	8.77895E-07	0.00028	0.00272
AC1:1	10	0.5784	6.08842E-06	0.00195	0.00105
	20	0.5445	5.73158E-06	0.00183	0.00117
	30	0.5350	5.63158E-06	0.00180	0.00120
	40	0.5224	5.49895E-06	0.00176	0.00124
	50	0.5058	5.32421E-06	0.00170	0.00130
AC1:4	10	0.5051	5.31684E-06	0.00170	0.00130
	20	0.5007	5.27053E-06	0.00169	0.00131
	30	0.4977	5.23895E-06	0.00168	0.00132
	40	0.4965	5.22632E-06	0.00167	0.00133
	50	0.4937	5.19684E-06	0.00166	0.00134
MC	10	0.7610	8.01053E-06	0.00256	0.00044
	20	0.7653	8.05579E-06	0.00258	0.00042
	30	0.7687	8.09158E-06	0.00259	0.00041
	40	0.7735	8.14211E-06	0.00260	0.00040
	50	0.7702	8.10737E-06	0.00259	0.00041
MAC 1:1	10	0.7645	8.04737E-06	0.00257	0.00043
	20	0.7126	7.50105E-06	0.00240	0.00060
	30	0.6866	7.22737E-06	0.00231	0.00069
	40	0.6466	6.80632E-06	0.00218	0.00082
	50	0.6049	6.36737E-06	0.00204	0.00096
MAC 1:4	10	0.6176	6.50105E-06	0.00208	0.00092
	20	0.5334	5.61474E-06	0.00180	0.00120
	30	0.4870	5.12632E-06	0.00164	0.00136
	40	0.4538	4.77684E-06	0.00153	0.00147
	50	0.4282	4.50737E-06	0.00144	0.00156

Table 3. 6: UV-Vis data for pH8 CSS with six different char precursors

pH8					
Precursors	Time (min)	Absorbance	Concentration (Mol/L)	Concentration (g/L) left in solution	Concentration (g/L) Adsorbed
C	10	0.1110	1.16842E-06	0.00037	0.00263

	20	0.1035	1.08947E-06	0.00035	0.00265
	30	0.1016	1.06947E-06	0.00034	0.00266
	40	0.0809	8.51579E-07	0.00027	0.00273
	50	0.0653	6.87368E-07	0.00022	0.00278
AC1:1	10	0.5726	6.02737E-06	0.00193	0.00107
	20	0.5118	5.38737E-06	0.00172	0.00128
	30	0.5150	5.42105E-06	0.00173	0.00127
	40	0.5110	5.37895E-06	0.00172	0.00128
	50	0.5098	5.36632E-06	0.00172	0.00128
AC1:4	10	0.4916	5.17474E-06	0.00166	0.00134
	20	0.4936	5.19579E-06	0.00166	0.00134
	30	0.4966	5.22737E-06	0.00167	0.00133
	40	0.5000	5.26316E-06	0.00168	0.00132
	50	0.5025	5.28947E-06	0.00169	0.00131
MC	10	0.5277	5.55474E-06	0.00178	0.00122
	20	0.5208	5.48211E-06	0.00175	0.00125
	30	0.5285	5.56316E-06	0.00178	0.00122
	40	0.5267	5.54421E-06	0.00177	0.00123
	50	0.4920	5.17895E-06	0.00166	0.00134
MAC 1:1	10	0.3873	4.07684E-06	0.00130	0.00170
	20	0.3512	3.69684E-06	0.00118	0.00182
	30	0.3153	3.31895E-06	0.00106	0.00194
	40	0.2469	2.59895E-06	0.00083	0.00217
	50	0.2041	2.14842E-06	0.00069	0.00231
MAC 1:4	10	0.1951	2.05368E-06	0.00066	0.00234
	20	0.1339	1.40947E-06	0.00045	0.00255
	30	0.0734	7.72632E-07	0.00025	0.00275
	40	0.0387	4.07368E-07	0.00013	0.00287
	50	0.0093	9.78947E-08	0.00003	0.00297

Table 3. 7: UV-Vis data for pH10 CSS with six different char precursors

pH10					
Precursors	Time (min)	Absorbance	Concentration (Mol/L)	Concentration (g/L) left in solution	Concentration (g/L) Adsorbed
C	10	0.1777	1.87053E-06	0.00060	0.00240
	20	0.1645	1.73158E-06	0.00055	0.00245
	30	0.1656	1.74316E-06	0.00056	0.00244
	40	0.1582	1.66526E-06	0.00053	0.00247
	50	0.1540	1.62105E-06	0.00052	0.00248
AC1:1	10	0.5157	5.42842E-06	0.00174	0.00126
	20	0.5163	5.43474E-06	0.00174	0.00126
	30	0.5200	5.47368E-06	0.00175	0.00125
	40	0.5220	5.49474E-06	0.00176	0.00124
	50	0.5245	5.52105E-06	0.00177	0.00123

AC1:4	10	0.5121	5.39053E-06	0.00172	0.00128
	20	0.5134	5.40421E-06	0.00173	0.00127
	30	0.5136	5.40632E-06	0.00173	0.00127
	40	0.5174	5.44632E-06	0.00174	0.00126
	50	0.5182	5.45474E-06	0.00174	0.00126
MC	10	0.7782	8.19158E-06	0.00262	0.00038
	20	0.7943	8.36105E-06	0.00267	0.00033
	30	0.7962	8.38105E-06	0.00268	0.00032
	40	0.7963	8.38211E-06	0.00268	0.00032
	50	0.8017	8.43895E-06	0.00270	0.00030
MAC 1:1	10	0.7107	7.48105E-06	0.00239	0.00061
	20	0.6945	7.31053E-06	0.00234	0.00066
	30	0.6740	7.09474E-06	0.00227	0.00073
	40	0.6229	6.55684E-06	0.00210	0.00090
	50	0.6149	6.47263E-06	0.00207	0.00093
MAC 1:4	10	0.5481	5.76947E-06	0.00185	0.00115
	20	0.5311	5.59053E-06	0.00179	0.00121
	30	0.5112	5.38105E-06	0.00172	0.00128
	40	0.4853	5.10842E-06	0.00163	0.00137
	50	0.4724	4.97263E-06	0.00159	0.00141

3.5 Proximity Analysis

3.5.1 Bulk Density

A glass cylinder (25 mL) was filled to a specified volume with a 1 mm – mesh grounded granulated sample and the cylinder was tapped for 1-2 minutes (Ekpete et al., 2017b). Table 3.8 shows value from bulk density experiment.

Table 3.8: Bulk density scaling

Glass Cylinder	Empty Glass Cylinder	Weight of dry sample	Weight of cylinder + Sample
25.0000 mL	43.6054 g	14.5192 g	58.1246 g

Figure 3.6: Bulk density scaling

The Bulk density was calculated using the formula:

$$\text{Bulk density} = \frac{\text{Mass of sample (dry) (g)}}{\text{Volume of measuring cylinder (mL)}}$$

3.5.2 Moisture Content

The thermal drying method was used in the determination of the moisture content of the samples. The uncarbonized sample was weighed in triplicate and placed in a clean, dried, and weighed crucible. The crucibles were placed in an oven at 105^0C to constant weight for 3 hr accordingly. The readings were taken every 3 hr for 15 hrs. The difference between the initial and final mass of the carbon represents the moisture content (Disco et al., 2017). Values were documented as seen in Table 3.9 and computed using the formula below:

Table 3.9: Moisture content data collected

Wt. (g)Empty crucible	**Sample Wt. (g)**	**Total Wt. (g)**	**Wt. (g), 3 hrs**	**Wt. (g), 6 hrs**	**Wt. (g), 9 hrs**	**Wt. (g), 12 hrs**	**Wt. (g), 15 hrs**
27.4857	2.0018	29.4871	29.3372	29.3360	29.3388	29.3339	29.3224
25.1915	2.0049	27.1992	27.0438	27.0478	27.0485	27.0485	27.0396
26.5613	2.0067	28.5676	28.4140	28.4168	28.4180	28.4117	28.3983

$$\text{Moisture\%} = 1 - \frac{\text{loss in weight on drying (g)}}{\text{Initial weight(g)}} \times 100$$

Where: $\text{loss in weight on drying (g)} = \text{weight of dried sample} - \text{weight of dish}$

Dish 1: $\text{Moisture\%} = 1 - \frac{29.3224\text{ g} - 27.4857\text{ g}}{2.0018\text{ g}} \times 100 = \mathbf{8.2475}\ \%$

Dish 2: $\text{Moisture\%} = 1 - \frac{27.0396\text{ g} - 25.1915\text{ g}}{2.0049\text{ g}} \times 100 = \mathbf{7.5564}\ \%$

Dish 3: $\text{Moisture\%} = 1 - \frac{28.3983\text{ g} - 26.5613\text{g}}{2.0067\text{ g}} \times 100 = \mathbf{8.4566}\ \%$

$$\text{Average value of the three dish values} = \frac{\text{dish 1} + \text{dish 2} + \text{dish 3}}{3} = \%$$

$$\text{Average value of the three dish values } \frac{8.2475\% + 7.5564\% + 8.4566\%}{3}$$

$$= \mathbf{8.0868}\%$$

3.5.3 Ash Content

Three crucibles were preheated to about 105^0 C, cooled in a desiccator, and weighed. The uncarbonized sample was weighed into each crucible and reweighed. The crucibles containing the samples were then placed in a muffle furnace and the temperature was allowed to rise to 575^0C for about 4 hr and allowed to cool in a desiccator to room temperature (30^0 C) and reweighed (Ekpete et al., 2017b). Figure 3.7 is the Muffle furnace used for the Ash Content preparation and Table 3.7 shows the data collected during the process.

Figure 3.7: Muffle furnace for Ash Content preparation

Table 3.10: Ash Content data collected

Wt. of crucible (g)	**Wt. of sample (g)**	**Total Wt. (g)**	**Ash content (g) after 4 hrs**
27.4857	2.0006	29.4863	27.5201
25.1915	2.0029	27.2004	25.2326
26.5613	2.0026	28.5639	26.5919

$$\text{Ash\%} = \frac{\text{Ash weight}}{\text{Oven dry weight(g)}} \times 100 = \%$$

Dish 1: $\text{Ash\%} = \frac{0.0344\ \text{g}}{2.0006\ \text{g}} \times 100 = \mathbf{1.7194}\%$

Dish 2: $\text{Ash\%} = \frac{0.0411\ \text{g}}{2.0029\ \text{g}} \times 100 = \mathbf{2.0520\%}$

Dish 3: $\text{Ash\%} = \frac{0.0306\ \text{g}}{2.0026\ \text{g}} \times 100 = \mathbf{1.5280\%}$

$$\text{Average value of the three dish values} = \frac{\text{dish 1} + \text{dish 2} + \text{dish 3}}{3} = \%$$

$$\text{Average value of the three dish values} = \frac{1.7194\% + 2.0520\% + 1.5280\%}{3} = \mathbf{1.7898\%}$$

3.5.4 Volatile Matter

The Uncarbonized samples used for moisture content were further used to conduct the volatile matter experiment. The samples in each crucible were reweighed. The crucibles containing the samples were then placed in a muffle furnace and the temperature was allowed to rise to 925^0C for about 7 minutes and allowed to cool in a desiccator to room temperature (30^0 C) and reweighed (Disco et al., 2017). The volatility was computed using the formula below and documented as shown in Table 3.11:

$$\text{Volatility (\%)} = \frac{\text{Initial weight (g)} - \text{Final Weight (g)}}{\text{Initial weight(g)}} \times 100$$

Table 3.11: Volatile Matter data collected

Wt. of empty crucible(g)	**Wt. of sample (g)**	**Total Wt. (g)**	**Crucible Wt. (g) + Volatile content (925^0C, after 7 min)**
27.4857	1.8367	29.3224	27.5030
25.1915	1.8445	27.0360	25.2101
26.5613	1.8370	28.3983	26.5668

3.6 Characterization Techniques

3.6.1 Fourier Transform Infrared (FT-IR) Spectrometer

FT-IR analysis was done using FT-IR (Model: Nicolet is5 Elmer, Manufacturer: Thermos Scientific) by using KBr pellets in the range of 400-4000 cm^{-1} at the spectral resolution of 4 cm^{-1} (Pongener et al., 2015). To prepare samples for the run, all samples were ground with KBr salt at a ratio of roughly 1/50 of all samples. After that, these samples were made as pellets (Hussein et al., 2015). FT-IR absorption spectrum was performed on the six precursors.

3.6.2 Scanning Electron Microscopy (SEM) and Energy Dispersive X-Ray Spectroscopy Analysis

Scanning electron microscopy coupled with energy-dispersive x-ray spectroscopy (SEM/EDX) were used to examine the morphology and the development of porosity of activated carbon prepared under the optimal conditions as well as to determine its elemental composition using (Manufacturer: Carl Zeiss, Model: Evo LS 10, made in Germany) instrument with an accelerating voltage of 20.00 kV. A Conductive tape was used to perfectly adhere the samples to the pin stubs surface. Dry air was sprayed on all the samples to remove loose particles before placing them in the sample stage. The samples image was taken at 20 µm Magnification.

CHAPTER FOUR
RESULTS AND DISCUSSION

4.1 Adsorption

The UV-Vis experiment shows the influence of various factors such as adsorbent preparation and concentration, initial dye concentration, temperature, the potential of hydrogen (pH) with respect to adsorbent contact time in the dye. From all indications, all conditioned pH dye solution from 4, 6, 7, 8, to 10 decreased with 17.01, 17.64, 28.48, 24.48, and 52.42% respectively from the initial dye solution. However, as acidity decreased to neutral value, the conditioned dye concentration decreased. In contrast, as alkalinity increased, the conditioned dye concentration decreased drastically compared to acidity.

4.1.1 The pH4 Adsorption

As seen in Figure. 4.1, MAC1:4 - pH4 shows an appreciable decrease in dye concentration. The percentage of initial dye concentration removed decreased by 97, 93, and 92% with an increase in contact time, and the amount of dye adsorbed (g/L) increased to 100% with an increase in contact time. Each peak as seen in the graphs indicates the limit of adsorption for each precusors considered.

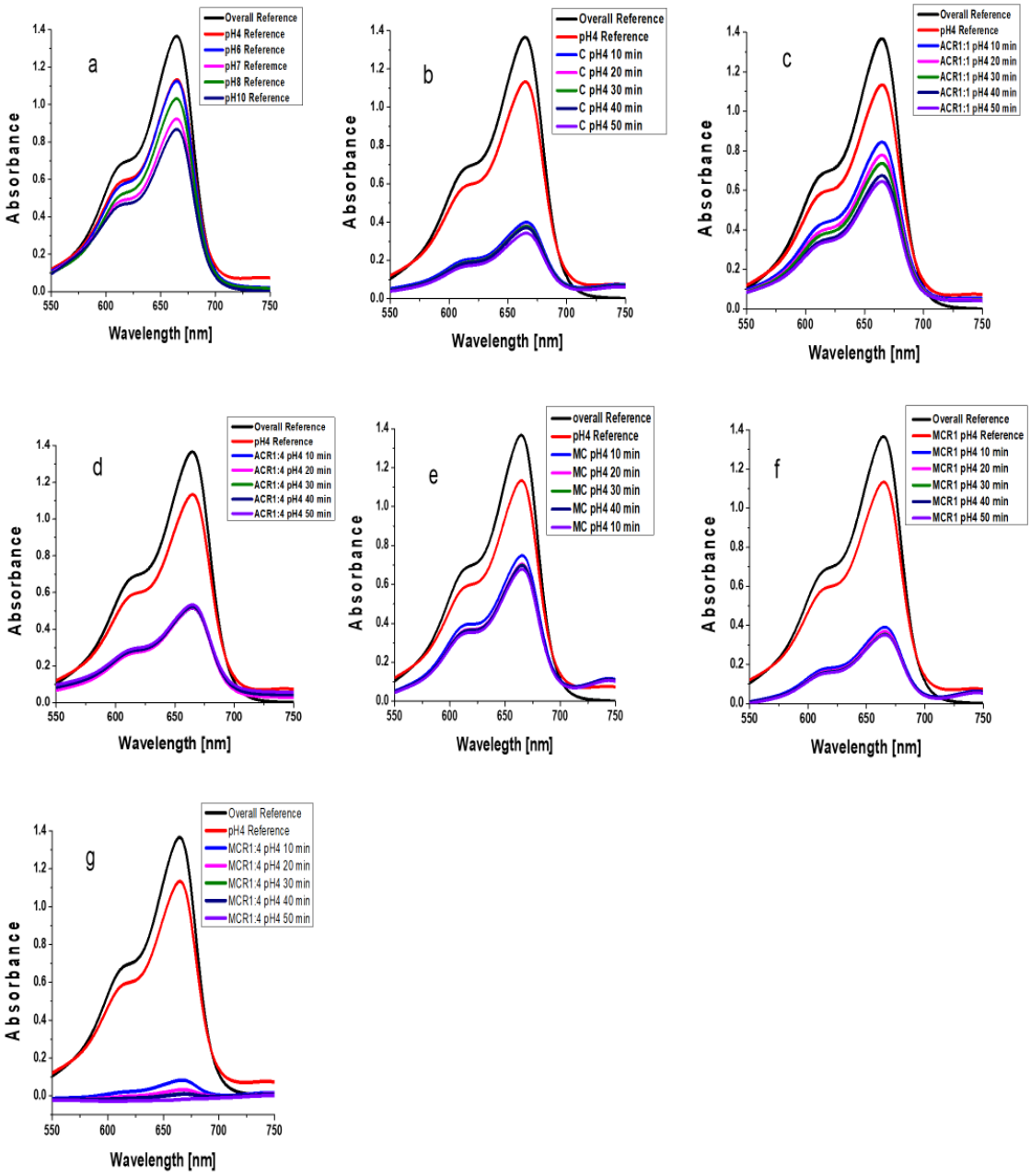

Figure 4.1: UV-Vis adsorption capacity of six different precursors (a) SS vs all CSS pH (4, 6, 7, 8, and 10) without char as references. (b) SS vs CSS pH4 reference vs CSS pH4 with Carbonized char. (c) SS vs CSS pH4 reference vs CSS pH4 with AC1:1 char. (d) SS vs CSS pH4 reference vs CSS pH4 with AC1:4 char. (e) SS vs CSS pH4 reference vs CSS pH4 with MC char. (f) SS vs CSS pH4 reference vs CSS pH4 with MAC1:1 char. (g) SS vs CSS pH4 reference vs CSS pH4 with MAC1:4 char.

4.1.2 The pH6 Adsorption

Just like in pH4, MAC1:4 - pH6 also shows a substantial decrease in dye concentration as seen in Figure 4.2. The graphical representations of MAC1:4 - pH6 solution show the percentage of initial dye concentration removed decreased by 89, 83, 78, 74, and 73 with an increase in contact time, and the amount of dye adsorbed (g/L) increased to 89% with an increase in contact time. Each peak as seen in the graphs indicates the limit of adsorption for each precusors considered.

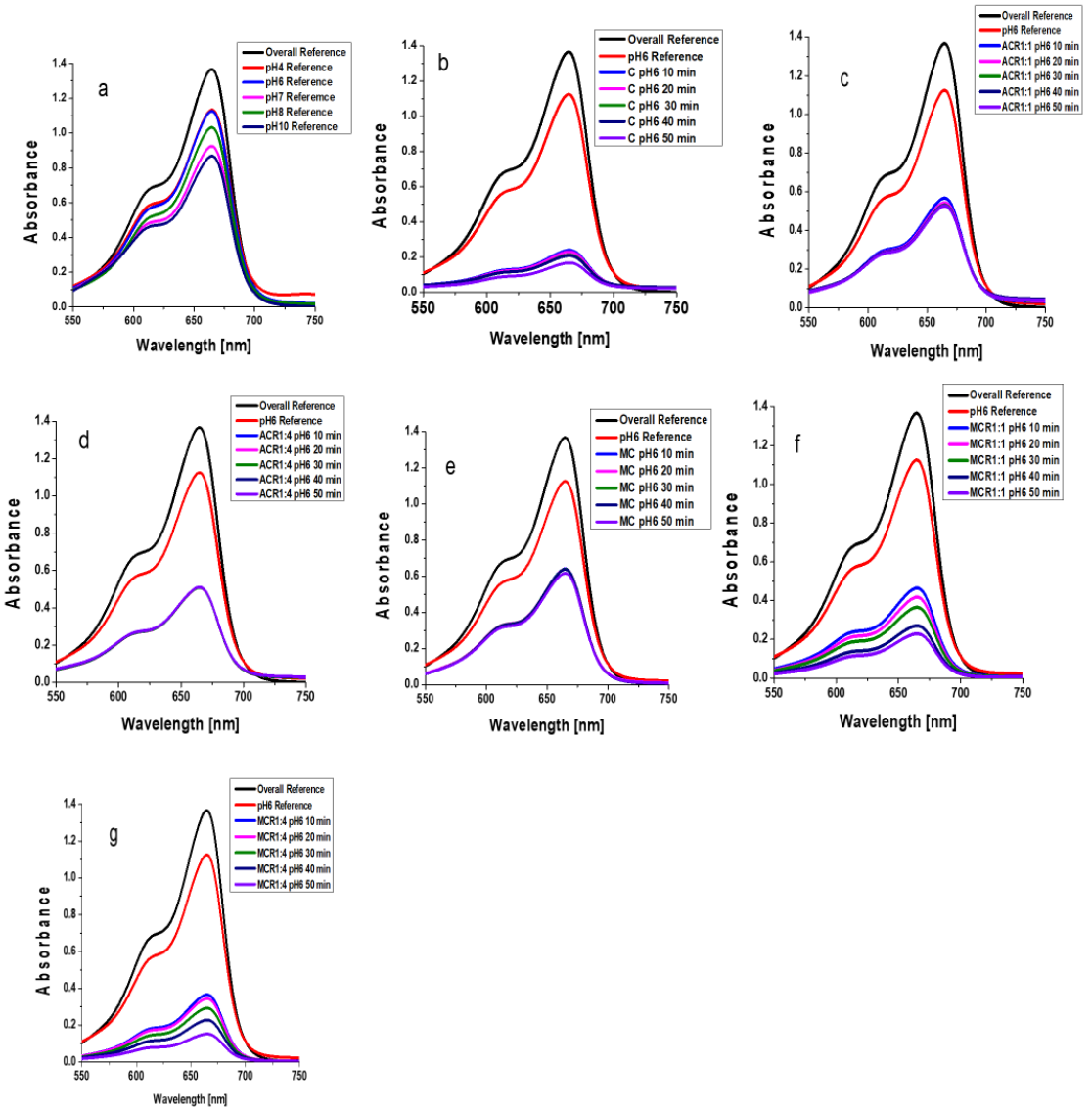

Figure 4.2: UV-VIS for adsorption capacity of six different precursors (a) SS vs all CSS pH (4, 6, 7, 8, and 10) without char as references. (b) SS vs CSS pH6 reference vs CSS pH6 with Carbonized char. (c) SS vs CSS pH6 reference vs CSS pH6 with AC1:1 char. (d) SS vs CSS pH6 reference vs CSS pH6 with AC1:4 char. (e) SS vs CSS pH6 reference vs CSS pH6 with MC char. (f) SS vs CSS pH6 reference vs CSS pH6 with

MAC1:1 char. (g) SS vs CSS pH6 reference vs CSS pH6 with MAC1:4 char.

4.1.3 The pH7 Adsorption

Like pH4 and pH6 where MAC1:4 shown a great dye adsorbate, CKCP - pH7 happens to be the best precursor with the following data: 93, 92, and 87% decrease in the initial dye concentration with an increase in contact time as seen in Figure 4.3. The amount of dye adsorbed (g/L) increased to 93% with an increase in contact time. Each peak as seen in the graphs indicates the limit of adsorption for each precusors considered.

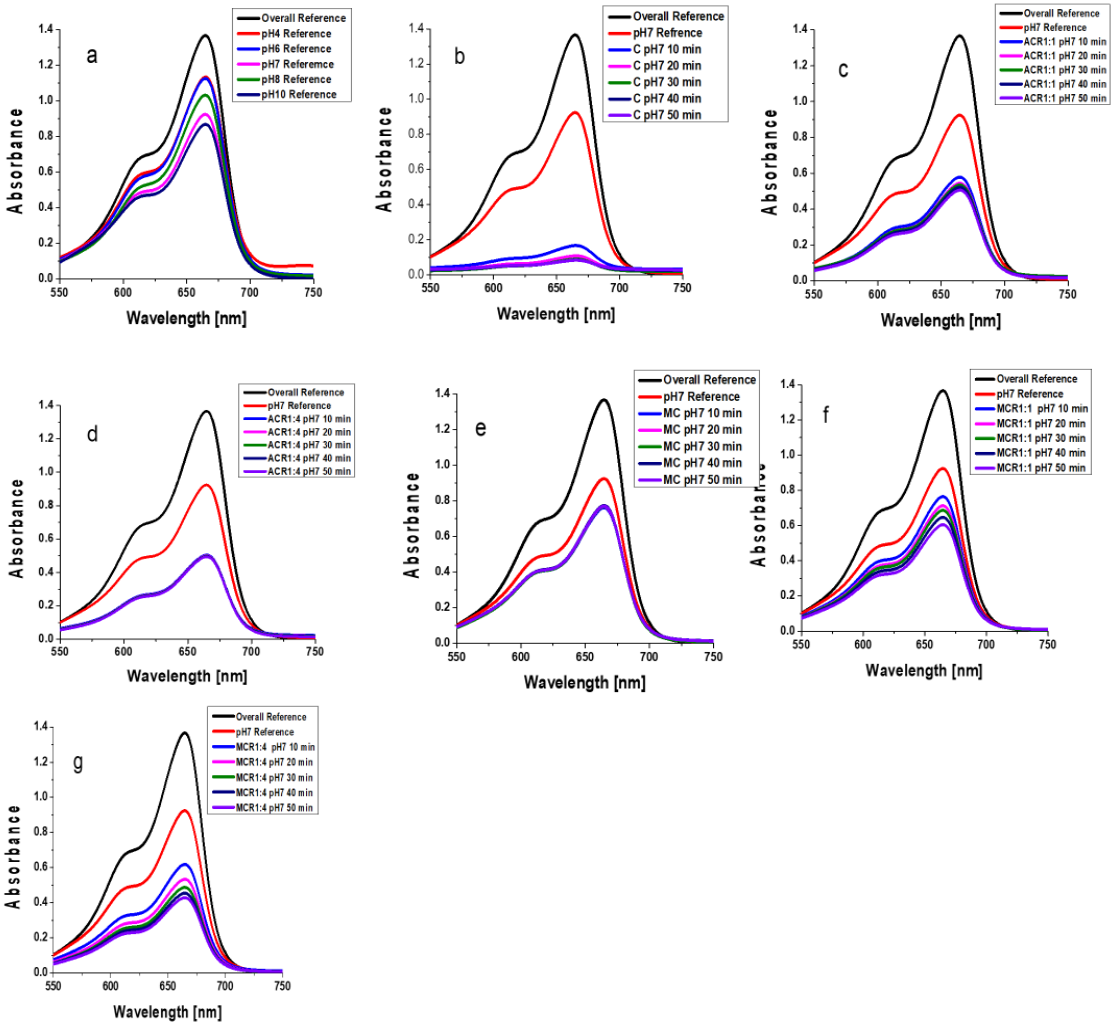

Figure 4.3: UV-Vis spectra; (a) SS vs all CSS pH (4, 6, 7, 8, and 10) without char as references. (b) SS vs CSS pH7 reference vs CSS pH7 with Carbonized char. (c) SS vs CSS pH7 reference vs CSS pH7 with AC1:1 char. (d) SS vs CSS pH7 reference vs CSS pH7 with AC1:4 char. (e) SS vs CSS pH7 reference vs CSS pH7 with MC char. (f) SS vs CSS pH7 reference vs CSS pH7 with MAC1:1 char. (g) SS vs CSS pH7 reference vs CSS pH7 with MAC1:4 char.

4.1.4 The pH 8 Adsorption

In Figure 4.4, the initial dye concentration decreased in the following order 99, 97, 94, 90 and 85% with an increase in contact time for MAC1:4 - pH8, similar to the trend in pH4 and pH6. The amount of dye adsorbed (g/L) increased by 99% with an increase in contact time. Each peak as seen in the graphs indicates the limit of adsorption for each precusors considered.

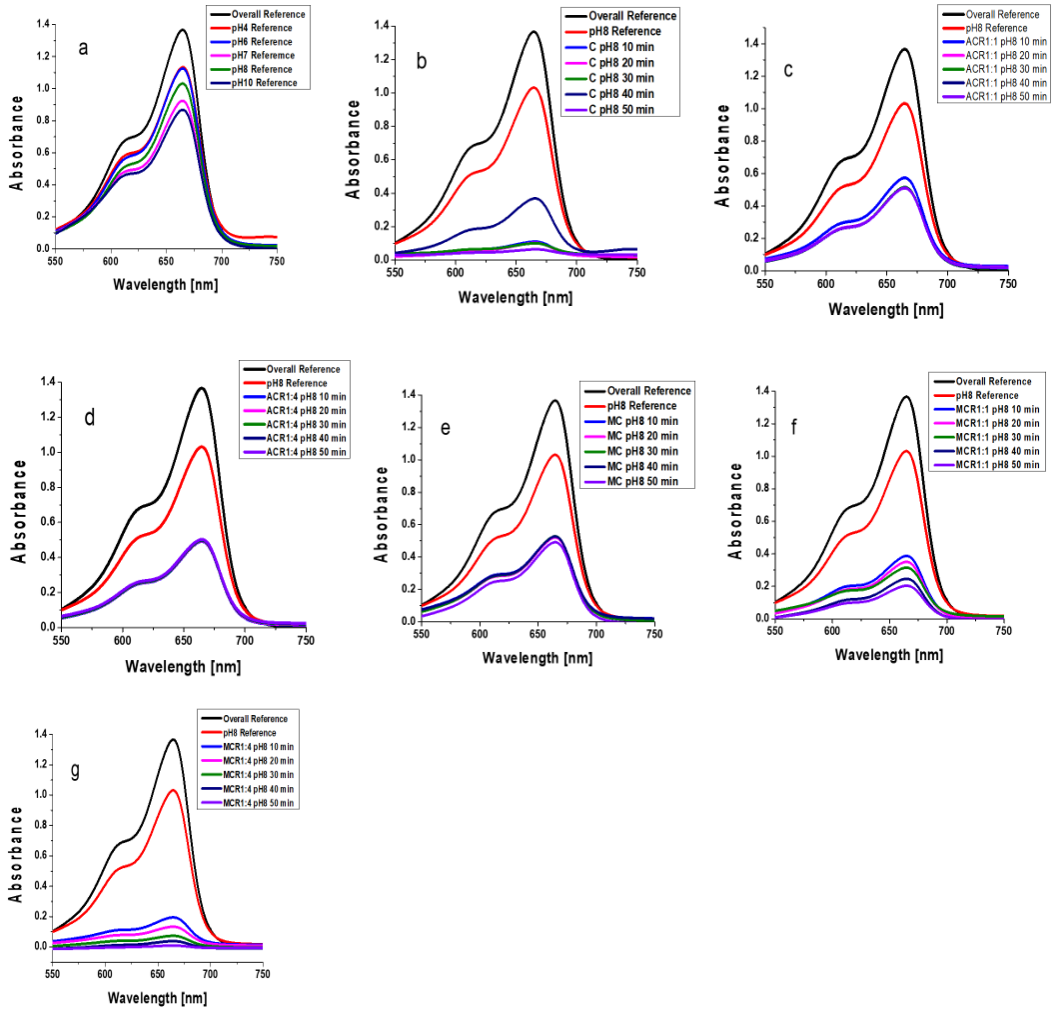

Figure 4.4: UV-Vis spectra (a) SS vs all CSS pH (4, 6, 7, 8, and 10) without char as references. (b) SS vs CSS pH8 reference vs CSS pH8 with Carbonized char. (c) SS vs CSS pH8 reference vs CSS pH8 with AC1:1 char. (d) SS vs CSS pH8 reference vs CSS pH8 with AC1:4 char. (e) SS vs CSS pH8 reference vs CSS pH8 with MC char. (f) SS vs CSS pH8 reference vs CSS pH8 with MAC1:1 char. (g) SS vs CSS pH8 reference vs CSS pH8 with MAC1:4 char.

4.1.5 The pH 10 Adsorption

Similar to pH7, in pH10 the percentage initial dye concentration removed decreased by 88, 87, and 86% with an increase in contact time, and the amount of dye adsorbed (g/L) increased by 88% with an increase in contact time for CKCP as seen in Figure 4.5. Each peak as seen in the graphs indicates the limit of adsorption for each precusors considered.

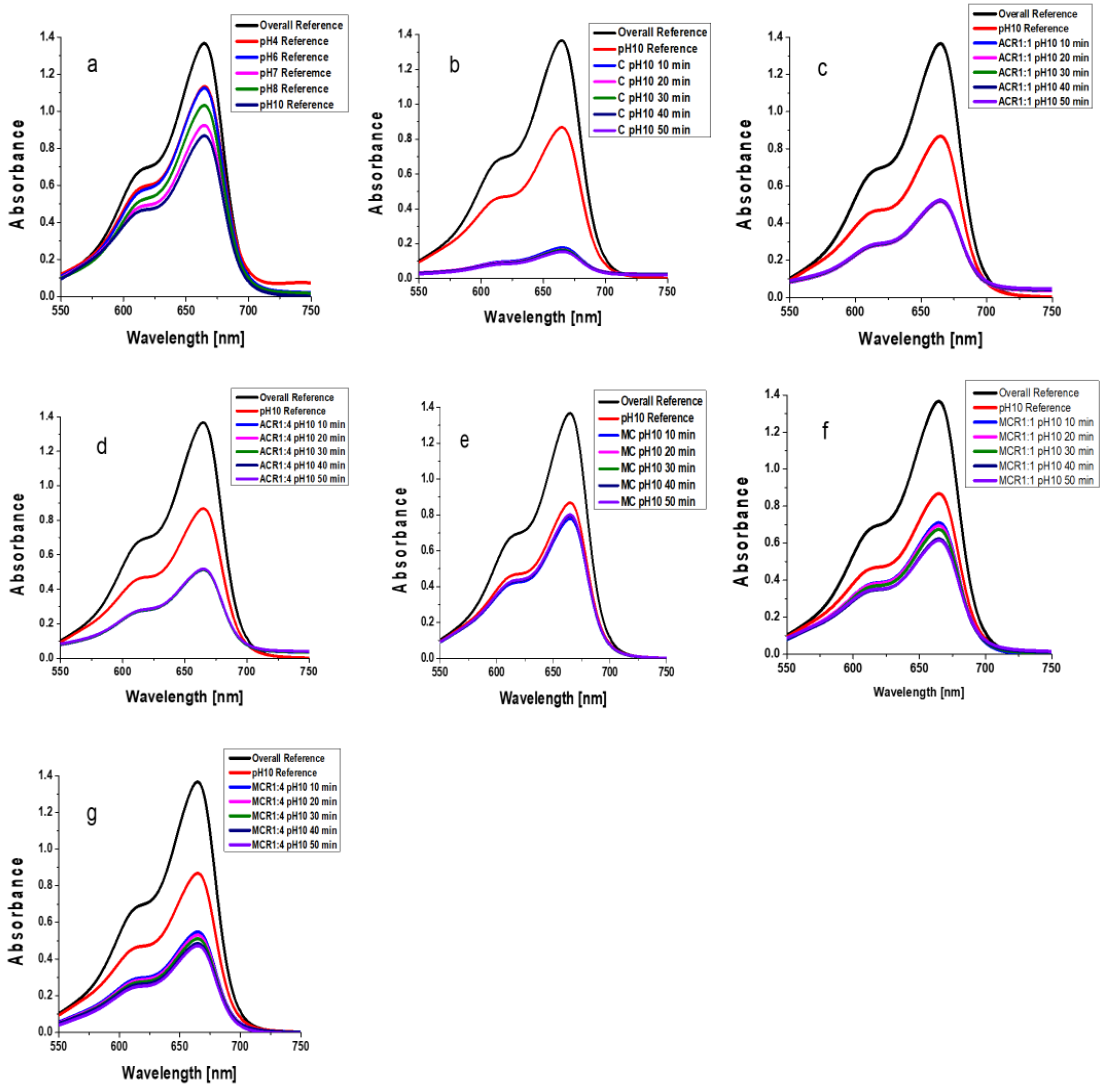

Figure 4.5: UV-VIS spetra for adsorption capacity of six different precursors; (a) SS vs all CSS pH (4, 6, 7, 8, and 10) without char as references. (b) SS vs CSS pH10 reference vs CSS pH10 with Carbonized char. (c) SS vs CSS pH10 reference vs CSS pH10 with AC1:1 char. (d) SS vs CSS pH10 reference vs CSS pH10 with AC1:4 char. (e) SS vs CSS pH10 reference vs CSS pH10 with MC char. (f) SS vs CS pH10

reference vs CSS pH10 with MAC1:1 char. (g) SS vs CSS pH10 reference vs CSS pH10 with MAC1:4 char.

4.2 SEM Imagining Characterization of Kcp Adsorption Precursors

SEM micrographs (Fig. 4.6) of all the precursors at a magnification of 20 µm respectively give a clear picture of the porosity of an adsorbent and also shows disorganized surface structures of different open pore sizes and shapes.

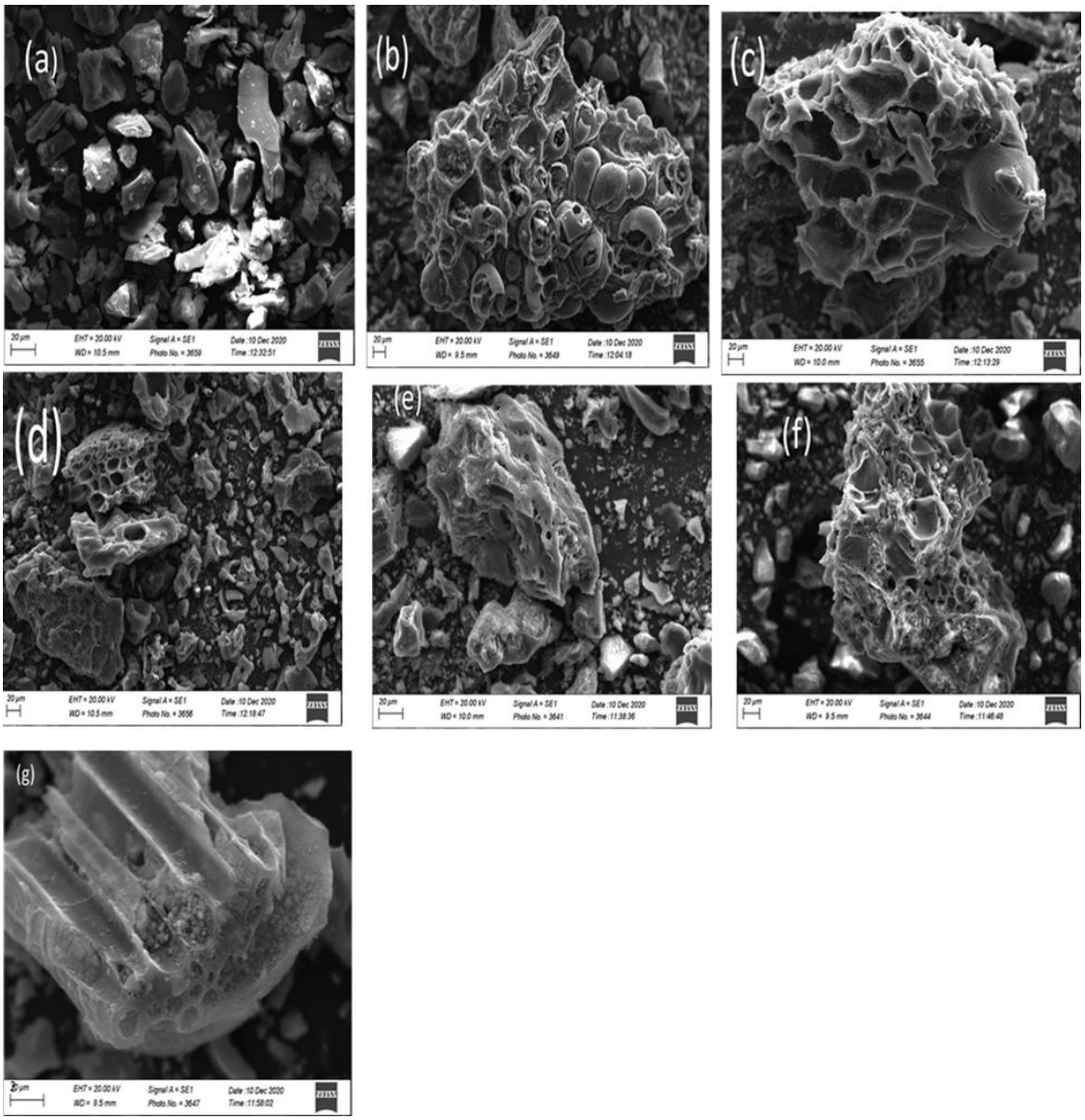

Figure 4.6: Scanning Electron Microscopy (SEM) micrographs of KCP samples taken at 20 µm magnifications (a) R-KCP, (b) Carb, (c) AC1:1, (d) AC1:4, (e) MC, (f) MAC1:1, and (g) MAC1:4.

The SEM micrographs of CKCP and MAC1:4 shown in Figure 4.6 (b and g) depicts the physical morphology of different preparation process. The CKCP shows a bubble-like

structure with different pore sizes and shapes, which is due to the removal of volatile compounds during carbonization (Kigozi et al., n.d.), while MAC1:4 reveals a hollow like structure with different pore sizes and shapes which may be due to high concentration of KOH treatment and presence of Fe(II) and Fe(III) filled into the hollow pores. RKCP shows a smooth irregular shape and sizes with no visible pores when compared to the other precursors, which is a result of no physical nor chemical treatment. AC1:1, AC1:4, MC, and MAC1:1 show disorganized surface structures of different open pore sizes and shapes which can be linked to the preparation condition (Pongener et al., 2015). The SEM images show that the higher the KOH activation the distribution of the more and effective developed pores on the surface of the precursor, thus leading to large surface area and porous structure of MAC1:4, which certified it a good adsorbent dependent of pH. The surface corrugation of CKCP is clearly visible from the SEM images which indicates that carbonization at 400^0 C without further physical or chemical activation processes is a preferable adsorbent based on the dye solution pH. Thus, the presence of different pores sizes in CKCP and MAC1:4 greatly influences the adsorption process.

4.3 FTIR Spectra Of The KCP Precursors

FT-IR analysis performed under ideal conditions revealed the presence of oxygen and aromatic structures in the precursors (Figure 4.7). The results indicating the oxidation and formation of functional groups at the surface of the materials. Absorption bands assigned to carboxyl, ethers, carbonyl, phenolic, and surface hydroxyl groups were used to detect surface chemical groups.

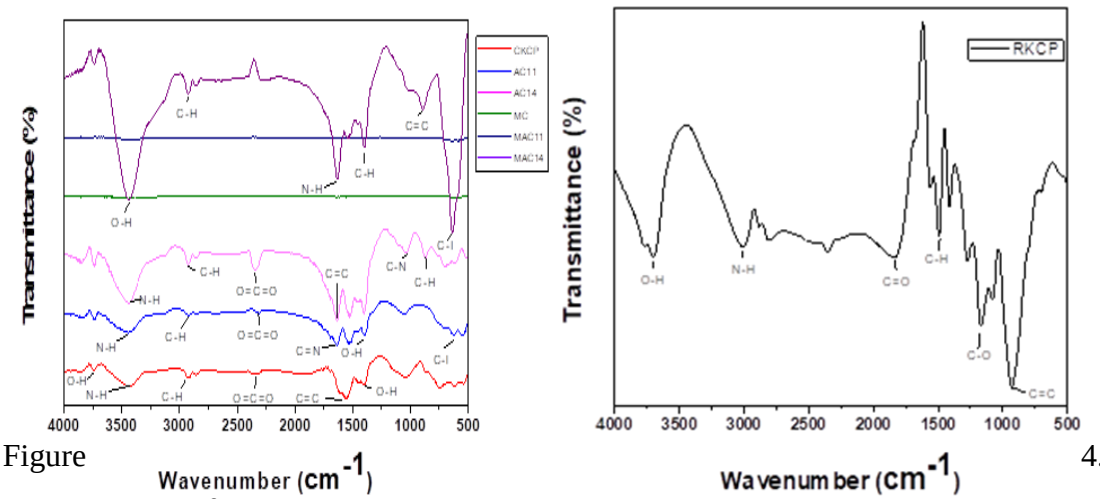

Figure 4.7: FT-IR spectra of; (a) six KCP precursors, and (b) Raw KCP.

The absorption of water molecules as a result of an O-H stretching mode of hydroxyl groups and adsorbed water results in a prominent peak at 3698 – 3434 cm^{-1} (Pongener et al., 2015). The N-H groups are associated with the big band at 3448–3247 cm^{-1} (Foo & Hameed, 2012). . A small peak at 2924 cm^{-1} could be attributed to methylene C-H stretch, while the band at 2855 - 2848 cm^{-1} is attributed to C-H stretch or N-CH3, which may be due to the association N of HNO3 with the surface carbon (Pongener et al., 2015). The existence of an amide group causes the peaks at 1648 - 1631 cm^{-1}. The C=C stretching in aromatics justifies the band at 1627 cm^{-1} (Salman, 2014). For carbon samples, the band at 1594 cm^{-1} has been unequivocally interpreted. The stretching vibrations of C=O moieties of conjugated systems such as diketone, keto ester, and keto-enol structures have been due to aromatic ring stretching coupled to strongly conjugated carbonyl groups (O'Reilly & Mosher, 1983). The C-O stretching bonds in phenols, ethers, lactones, and hydroxyl groups are visible and attributed to bands around 1174 - 1153 cm^{-1}. Alcoholic C-O stretching vibration is described by bands at 1033 cm^{-1}. Out of plane deformation vibrations of the C-H group in aromatic structures are characterized by bands below 930 – 916 cm^{-1} (Rao et al., 2011). As shown in Figure 4.7, the CKCP and MAC1:4 precursors possess lower transmittance than the other four precursors showing that CKCP and MAC1:4 have higher absorbance capacity than the other four samples.

4.4 Energy Dispersive X-Ray Spectroscopy (EDX)

EDX analytical technique was used for elemental analysis of the samples. The EDX analysis result and the corresponding spectra are shown in Figure 4.8. The RKCP, CKCP, AC1:1, AC1:4, MC, MAC1:1, and MAC1:4 respectively. The carbon content is 69.55, 76.45, 83.62, 75.28, 0.04, 48.44 and 35.60 % respectively while iron dominated all the MC, MAC1:1, AND MAC1:4 samples in the order: 92.88, 17.25, and 25.81 % as expected due to the presence of Fe(II) and Fe(III) used in the preparation of the magnetic samples.

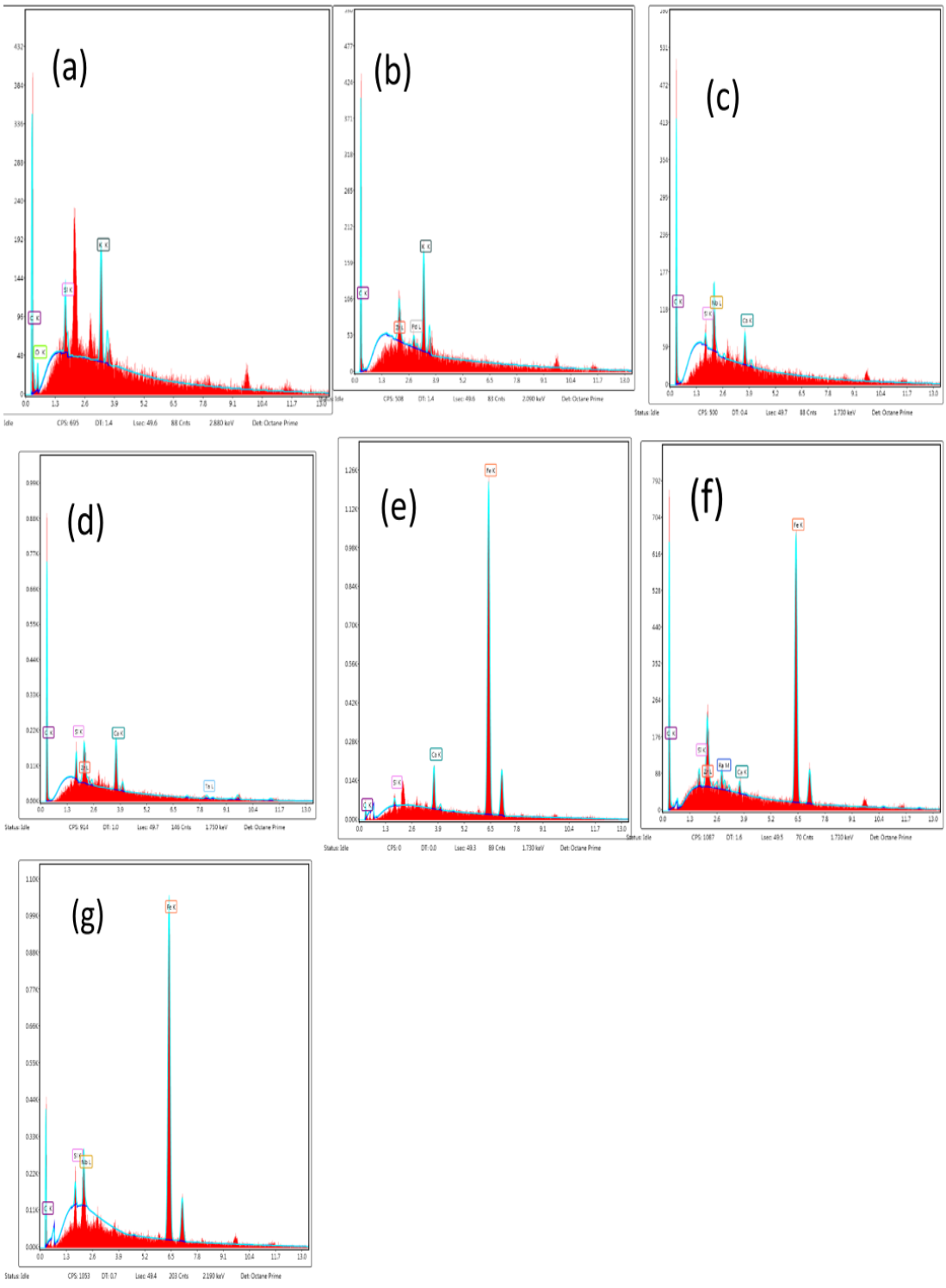

Figure 4.8: Energy-Dispersive X-ray spectroscopy (EDX) of KCP revealing the spectra and elemental analysis in: (a) R-KCP, (b) CKCP, (c) AC1:1, (d) AC1:4, (e) MC, (f) MAC1:1, and (g) MAC1:4.

Table 4.1: EDX elemental analysis of all precursors

Element in RKCP	Weight %	Atomic %
C K	69.55	81.14

Element in CKCP	Weight %	Atomic %
C K	76.45	92.39

Element in AC1:1	Weight %	Atomic %
C K	83.62	96.34

Element in AC1:4	Weight %	Atomic %
C K	75.28	93.49

Element in MC	Weight %	Atomic %
C K	0.04	0.17
Fe K	95.1	92.88

Element in MAC1:1	Weight %	Atomic %
C K	48.44	81.55
Fe K	47.63	17.25

Element in MAC 1:4	Weight %	Atomic %
C K	35.6	72.28
Fe K	59.12	25.81

4.5

Factors Affecting Adsorption of Dyes

The adsorption process of KCP derived adsorbate was affected by the following factors: the initial dye concentration, the solution pH, activation ratio, the contact time between the adsorbent and the adsorbate. The effects of these parameters on adsorption capability have been studied by several researchers. When conducting lab-scaled experiments, optimization of such conditions should be considered to ensure better adsorption capability.

4.5.1 Effect of Initial Dye Concentration

As observed in the overall reference MB dye stock solution, the initial MB concentration produces an increase in adsorption of the condition dye solution. The effect of initial dye concentration on the removal of dyes depends on the immediate relation between the concentration of the dye and the available sites on an adsorbent surface. Different percentages of dye removal for all the KCP precursors displayed the same attribute of decrease with an increase in the initial dye concentration, although the amount of dye adsorbed (g/L) increased with increased dye concentration. This observation can be related to the fact that when the concentration gradient between the aqueous solution and the solid phase increases (El Maguana et al., 2018). Moreover, the increase in the initial concentration increases the contact probability between MB and carbon precursors (El Maguana et al., 2019; Haddad et al., 2015). It can also be due to the high driving force created by the high initial concentration to overcome all mass transfer resistance of the dye between the aqueous and solid phases (A. Ahmad et al.,

2009; Chikri et al., 2020b).

4.5.2 Effect of the Solution pH

The overall reference and the conditioned pH dye solutions indicate as acidity decreases to neutral value, the conditioned dye concentration decreases. In contrast, as alkalinity increases, the conditioned dye concentration decreases drastically compared to acidity.

The pH of a medium will control the magnitude of electrostatic charges which are imparted by the ionized dye molecules. As a result, the rate of adsorption will vary with the pH of an aqueous medium (Tripathi, 2013). As seen in Figures 4.1 to 4.5, different adsorbent preparation condition was observed, Carbonized (pH7 and pH10) and MAC1:4 (pH4, pH6, and pH8) precursor preparation has the best dye adsorbate compared to AC1:1, AC1:4, and MB. As related by other researchers, at low pH solution, the positive charge on the solution interface will increase and the adsorbent surface appears positively charged. As a result, the removal efficiency for cationic dye will decrease, while the removal percentage for anionic dyes will increase. In contrast, at high pH solution, the positive charge at the solution interface decreases, and the adsorbent surface appears negatively charged, which increases cationic dye adsorption and a decrease in anionic dye adsorption (Chikri et al., 2020b; Tripathi, 2013),

4.5.3 Effect of Activation Ratio

The MAC1:4 (C: KOH) and CKCP displayed excellent dispersion, convenient separation, and high adsorption capacity Removal efficiency increases with an increase in activation ratio for solution pH 4, 6, and 8 compared to MAC1:1, AC1:1, and AC1:4 in the chemical impregnation activation categories. This is due to initial pores been developed through carbonization, activation enhances further development of pores. This produces an ordering of the structure with highly porous activated carbon for improved performance on the adsorption process. The SEM image in Figure 4.6 shows the micrographs effect of the C: KOH ratio. Similarly, (Osman & Yüksel, 2018) studied the removal efficiency of three activated carbon samples with different activation ratios and the activated carbon with the highest ratio has the highest removal efficiency. However, the type of pores to be produced depends on different activation conditions whereby activation ratio is very potential for micropores production when chemical activation is used. Production of micropores increases with an increase in activation ratio. (Juma et al., 2020; Sudaryanto et al., 2006).

4.5.4 Effect of contact time

In the first 10 min, the adsorption process was very rapid and the rate of removal was higher; this can be attributed to the presence of a larger surface area presented by the adsorbent and the availability of free active sites at the beginning time for the adsorption of the adsorbate. Towards 20 to 40 min, the adsorption rate gradually becomes relatively slower with the increase of contact time and, at some point in time, reached a constant value where no more adsorbate was removed from the solution. Finally, at about 40 to 50 min, the process attains the saturation phase as observed on the graphs in Figures 4.1 to 4.5. At that time, the lack of free active sites on the adsorbent was the reason behind this behavior (Chikri et al., n.d.; Sulyman et al., 2017). As a result of many experiments performed by different scientists, is being observed that the dye removal efficiency on an adsorbent varies with time, variation may be of both nature either positive or negative which means dye removing efficiency of an adsorbent may increase or decrease with a course of time. As recorded by (Tripathi, 2013), Some graphical data from the experiment performed on an orange peel, neem leaves, banana peel, activated carbon and tamarind fruit shell, dye removing efficiency of an adsorbent may increase or decrease with time.

4.6 Proximity Analysis

The data obtained from proximate analysis (moisture content, ash, volatile matter, and bulk density) of other biomass samples and that of this study is presented in Table 4.1

Table 4.1: Characteristics of biochar from different biomass

Biomass	Moisture Content Wt%	Ash Content Wt%	Volatile matter Wt%	Bulk Density g/ml	Reference
Tamarind seed	1.14 ± 0.07	1.65 ± 0.4	67.64 ± 1.30	-	(Mopoung et al., 2015)
Palm Shell	8.0	1.1	72.5	-	(Daud et al., 2000)
Rice Straw	7.20	15.40	62.40	-	(Narzari & Bordoloi, 2015)
Coconut Shell	4.40	0.70	80.20	-	
Beans Husk	8.50	3.5	-	0.41	(Evwierhoma et al., 2018)
Kentucky coffee pods	8.08	1.78	99.25	0.58	This study

CHAPTER FIVE
CONCLUSION AND RECOMMENDATION

5.1 Conclusion

There has been a high increase in production and utilization of dyes in the last few decades resulting in a big threat of pollution. Agricultural wastes and biomass are known to be good dye adsorbing agents. It can be concluded that the agricultural wastes are effective in their natural forms with physical and chemical modifications. The Langmuir model is usually used to evaluate the adsorption capacity of the agricultural wastes as adsorbents and most studies of dye adsorption by agricultural solid wastes. Technical improvements in preparing and utilizing adsorbents in most cases, these adsorbents require a treatment process to enhance their capability for dye removal. This research makes a comparison between the Carbonization, Activation Carbon, and Magnetic Activation Carbon process of Kentucky Coffee pods.

According to (Katheresan et al., 2018), five factors can affect the rate of adsorption which are the dye concentration, the solution pH, the adsorbent dosage, contact time, and the temperature of the solution. It was also reported by (Chikri et al., 2020a) from is research that: (i) The rate of adsorption increases with increasing of adsorbent dosage and vice versa (ii) The rate of adsorption can be high if contact time is long and vice versa (iii) High rate of adsorption is found if dye concentration is low and vice versa (iv) Low rate of adsorption is obtained when pH is low and vice versa (v) Low rate of adsorption is obtained if temperature is too low or too high. The MAC1:4 is a good precursor for pH 4, 6 and 8 value while preferably CKCP is the best precursor for pH 7 and 10. The effect of concentration (increase in activation ratio) was felt on the type of pores produced for better adsorption on MAC1:4. More so, increase in contact time result showed a higher adsorption capacity, this leads to lack of free active sites on the adsorbent was the reason behind the decrease in concentration of dye in the solution.

Carbonized (pH7 and pH10) and MAC1:4 (pH4, pH6, and pH8) precursor preparation had the best dye adsorbate compared to AC1:1 and AC1:4. This is greatly associated with the dye solution pH, adsorbent preparation conditions, contact time, and temperature of the solution, and high volatility value. This research also exhibits the factors affecting the rate of adsorption reported by (Katheresan et al., 2018) and (Chikri

et al., 2020a)

5.2 Recommendation

This study was limited to characterization using FT-IR, SEM, and EDX due to availability of equipment. Future research is proposed to look into Thermodynamics, Kinetic studies characterization such as XRD, XRF, TGA, and BET to give in-depth analyses on the considered precursors.

REFERENCES

Ahmad, A., Rafatullah, M., Sulaiman, O., Ibrahim, M. H., & Hashim, R. (2009). Scavenging behaviour of meranti sawdust in the removal of methylene blue from aqueous solution. *Journal of Hazardous Materials*, *170*(1), 357–365. https://doi.org/10.1016/j.jhazmat.2009.04.087

Ahmad, Asif, & Azam, T. (2019). Water Purification Technologies. In *Bottled and Packaged Water* (pp. 83–120). Elsevier. https://doi.org/10.1016/b978-0-12-815272-0.00004-0

Ahmad, M., Lee, S. S., Dou, X., Mohan, D., Sung, J. K., Yang, J. E., & Ok, Y. S. (2012). Effects of pyrolysis temperature on soybean stover- and peanut shell-derived biochar properties and TCE adsorption in water. *Bioresource Technology*, *118*, 536–544. https://doi.org/10.1016/j.biortech.2012.05.042

Aznar, J. S. (2011). *Characterization of activated carbon produced from coffee residues by chemical and physical activation*. *March*.

Bautista, P., Mohedano, A. F., Casas, J. A., Zazo, J. A., & Rodriguez, J. J. (2011). Highly stable Fe/γ-Al2O3 catalyst for catalytic wet peroxide oxidation. *Journal of Chemical Technology and Biotechnology*, *86*(4), 497–504. https://doi.org/10.1002/jctb.2538

Bayazit, Ş. S., & Kerkez, Ö. (2014). Hexavalent chromium adsorption on superparamagnetic multi-wall carbon nanotubes and activated carbon composites. *Chemical Engineering Research and Design*, *92*(11), 2725–2733. https://doi.org/10.1016/j.cherd.2014.02.007

Biniak, S., Świątkowski, A., & Pakuła, M. (2017). *Chemistry and Physics of Carbon A Series of Advances*. *January 2001*.

Bjerregaard, P. (2008). Case reports. *Journal of Electrocardiology*, *41*(2), 83. https://doi.org/10.1016/j.jelectrocard.2007.12.009

Cazetta, A. L., Pezoti, O., Bedin, K. C., Silva, T. L., Paesano Junior, A., Asefa, T., & Almeida, V. C. (2016). Magnetic Activated Carbon Derived from Biomass Waste by Concurrent Synthesis: Efficient Adsorbent for Toxic Dyes. *ACS Sustainable Chemistry and Engineering*, *4*(3), 1058–1068. https://doi.org/10.1021/acssuschemeng.5b01141

Chikri, R., Elhadiri, N., Benchanaa, M., & El maguana, Y. (2020a). Efficiency of Sawdust as Low-Cost Adsorbent for Dyes Removal. *Journal of Chemistry*, *2020*, 1–17. https://doi.org/10.1155/2020/8813420

Chikri, R., Elhadiri, N., Benchanaa, M., & El maguana, Y. (2020b). Efficiency of Sawdust as Low-Cost Adsorbent for Dyes Removal. *Journal of Chemistry*, *2020*, 1–17. https://doi.org/10.1155/2020/8813420

Chikri, R., Elhadiri, N., Benchanaa, M., & Maguana, Y. El. (n.d.). *Efficiency of Sawdust as Low-Cost Adsorbent for Dyes Removal*. Retrieved February 27, 2021, from https://www.hindawi.com/journals/jchem/2020/8813420/

Considine, R., Denoyel, R., Pendleton, P., Schumann, R., & Wong, S. H. (2001). The influence of surface chemistry on activated carbon adsorption of 2-methylisoborneol from aqueous solution. *Colloids and Surfaces A: Physicochemical and Engineering Aspects*, *179*(2–3), 271–280. https://doi.org/10.1016/S0927-7757(00)00647-6

Danyuo, Y., Arthur, E. K., Azeko, S. T., Asuo, I. M., Danyuo, Y., Azeko, S. T., & Obayemi, J. D. (2014). Design of Locally Produced Activated Carbon Filter from Agricultural Waste for Water Purification. *International Journal of Engineering Research & Technology*, *3*(6), 531–540.

Daud, W. M. A. W., Ali, W. S. W., & Sulaiman, M. Z. (2000). Effects of carbonization temperature on pore development in palm-shell-based activated carbon. *Carbon*, *38*(14), 1925–1932. https://doi.org/10.1016/S0008-6223(00)00028-2

Demarchi, C. A., Michel, B. S., Nedelko, N., Ślawska-Waniewska, A., Dłużewski, P., Kaleta, A., Minikayev, R., Strachowski, T., Lipińska, L., Dal Magro, J., & Rodrigues, C. A. (2019). Preparation, characterization, and application of magnetic activated carbon from termite feces for the adsorption of Cr(VI) from aqueous solutions. *Powder Technology*, *354*, 432–441. https://doi.org/10.1016/j.powtec.2019.06.020

Derakhshan, Z., Baghapour, M. A., Ranjbar, M., & Faramarzian, M. (2013). Adsorption of Methylene Blue Dye from Aqueous Solutions by Modified Pumice Stone: Kinetics and Equilibrium Studies. *Health Scope*, *2*(3), 136–144. https://doi.org/10.17795/jhealthscope-12492

Dhananasekaran, S., Palanivel, R., & Pappu, S. (2016). Adsorption of Methylene Blue, Bromophenol Blue, and Coomassie Brilliant Blue by α-chitin nanoparticles. *Journal of Advanced Research*, *7*(1), 113–124. https://doi.org/10.1016/j.jare.2015.03.003

Disco, Y., Mahanta, P., & Bora, U. (2017). Comprehensive characterization of lignocellulosic biomass through proximate , ultimate and compositional analysis for bioenergy production. *Renewable Energy*, *103*, 490–500. https://doi.org/10.1016/j.renene.2016.11.039

Ekpete, O. A., Marcus, A. C., & Osi, V. (2017a). *Preparation and Characterization of Activated Carbon Obtained from Plantain (Musa paradisiaca) Fruit Stem*. https://doi.org/10.1155/2017/8635615

Ekpete, O. A., Marcus, A. C., & Osi, V. (2017b). Preparation and Characterization of Activated Carbon Obtained from Plantain (Musa paradisiaca) Fruit Stem. *Journal of Chemistry*, *2017*(January). https://doi.org/10.1155/2017/8635615

El Maguana, Y., Elhadiri, N., Bouchdoug, M., Benchanaa, M., & Boussetta, A. (2018). Optimization of Preparation Conditions of Novel Adsorbent from Sugar Scum Using Response Surface Methodology for Removal of Methylene Blue. *Journal of Chemistry*, *2018*. https://doi.org/10.1155/2018/2093654

El Maguana, Y., Elhadiri, N., Bouchdoug, M., Benchanaa, M., & Jaouad, A. (2019). Activated Carbon from Prickly Pear Seed Cake: Optimization of Preparation Conditions Using Experimental Design and Its Application in Dye Removal. *International Journal of Chemical Engineering*, *2019*. https://doi.org/10.1155/2019/8621951

Evwierhoma, E. T., Madubiko, O. D., & Jaiyeola, A. (2018). Preparation and characterization of activated carbon from bean husk. *Nigerian Journal of Technology*, *37*(3), 674. https://doi.org/10.4314/njt.v37i3.17

Fazal-Ur-Rehman, M. (2019). *Methodological trends in preparation of activated carbon from local sources and their impacts on production: A review*. *June*. https://doi.org/10.31221/osf.io/5m7fp

Fierro, V., Izquierdo, M. T., Schuurman, Y., Rubio, B., & Mirodatos, C. (2002). A novel approach for characterising carbon catalysts by TAP experiments. *Studies in Surface Science and Catalysis*, *144*, 255–260. https://doi.org/10.1016/s0167-2991(02)80142-2

Foo, K. Y., & Hameed, B. H. (2012). Coconut husk derived activated carbon via microwave induced activation: Effects of activation agents, preparation parameters and adsorption performance. *Chemical Engineering Journal*, *184*, 57–65. https://doi.org/10.1016/j.cej.2011.12.084

Gao, X., Zhang, Y., Dai, Y., & Fu, F. (2016). High-performance magnetic carbon materials in dye removal from aqueous solutions. *Journal of Solid State Chemistry*, *239*, 265–273. https://doi.org/10.1016/j.jssc.2016.05.001

Geçgel, Ü., Özcan, G., & Çağla Gürpınar, G. (2013). Removal of Methylene Blue from Aqueous Solution by Activated Carbon Prepared from Pea Shells (Pisum sativum). *Journal of Chemistry*, *2013*. https://doi.org/10.1155/2013/614083

Getachew, T., Hussen, A., & Rao, V. M. (2015). Defluoridation of water by activated carbon prepared from banana (Musa paradisiaca) peel and coffee (Coffea arabica) husk. *International Journal of Environmental Science and Technology*, *12*(6), 1857–1866. https://doi.org/10.1007/s13762-014-0545-8

Gilman, E. F., & Watson, D. G. (2021). *Gymnocladus dioicus: Kentucky Coffeetree 1*. http://edis.ifas.ufl.edu.

Gupta, B. S., & Afshari, M. (2009). Tensile failure of polyacrylonitrile fibers. In *Handbook of Tensile Properties of Textile and Technical Fibres* (pp. 486–528). Elsevier Inc. https://doi.org/10.1533/9781845696801.2.486

Haddad, K., Jellali, S., Jaouadi, S., Benltifa, M., Mlayah, A., & Hamzaoui, A. H. (2015). Raw and treated marble wastes reuse as low cost materials for phosphorus removal from aqueous solutions: Efficiencies and mechanisms. *Comptes Rendus Chimie*, *18*(1), 75–87. https://doi.org/10.1016/j.crci.2014.07.006

Haham, H., Grinblat, J., Sougrati, M. T., Stievano, L., & Margel, S. (2015). Engineering of iron-based magnetic activated carbon fabrics for environmental remediation. *Materials*, *8*(7), 4593–4607. https://doi.org/10.3390/ma8074593

Han, S., Zhao, F., Sun, J., Wang, B., Wei, R., & Yan, S. (2013). Removal modified of p-nitrophenol from aqueous activated carbon solution by magnetically. *Journal of Magnetism and Magnetic Materials*, *341*, 133–137. https://doi.org/10.1016/j.jmmm.2013.04.018

Heidarinejad, Z., Dehghani, M. H., Heidari, M., Javedan, G., Ali, I., & Sillanpää, M. (2020). Methods for preparation and activation of activated carbon: a review. In *Environmental Chemistry Letters* (Vol. 18, Issue 2, pp. 393–415). Springer. https://doi.org/10.1007/s10311-019-00955-0

Hussein, F. H., Halbus, A. F., Lafta, A. J., & Athab, Z. H. (2015). Preparation and characterization of activated carbon from iraqi khestawy date palm. *Journal of Chemistry*, *2015*. https://doi.org/10.1155/2015/295748

Inagaki, M., Kang, F., Toyoda, M., & Konno, H. (2014a). Carbonization Under Pressure. In *Advanced Materials Science and Engineering of Carbon* (pp. 67–85). Elsevier. https://doi.org/10.1016/b978-0-12-407789-8.00004-1

Inagaki, M., Kang, F., Toyoda, M., & Konno, H. (2014b). Template Carbonization. In *Advanced Materials Science and Engineering of Carbon* (pp. 133–163). Elsevier. https://doi.org/10.1016/b978-0-12-407789-8.00007-7

Jayajothi, C., Senthamilselvi, D. M. M., Arivoli, S., & Muruganantham, N. (2017). Kinetic, Thermodynamic and Isotherm Studies on the Removal of Methylene Blue Dye using Acid Activated Glossocardia linearifolia Stem. *IOSR Journal of Applied Chemistry*, *10*(06), 30–37. https://doi.org/10.9790/5736-1006013037

Juma, G., Machunda, R., & Pogrebnaya, T. (2020). Performance of Sweet Potato's Leaf-Derived Activated Carbon for Hydrogen Sulphide Removal from Biogas. *Journal of Energy*, *2020*, 1–10. https://doi.org/10.1155/2020/9121085

Katheresan, V., Kansedo, J., & Lau, S. Y. (2018). Efficiency of various recent wastewater dye removal methods: A review. In *Journal of Environmental Chemical Engineering* (Vol. 6, Issue 4, pp. 4676–4697). Elsevier Ltd. https://doi.org/10.1016/j.jece.2018.06.060

Kigozi, M., Kali, R., Bello, A., Padya, B., Mong Kalu-Uka, G., Wasswa, J., Jain, P. K., Onwualu, P. A., & Dzade, N. Y. (n.d.). *materials Modified Activation Process for Supercapacitor Electrode Materials from African Maize Cob*. https://doi.org/10.3390/ma13235412

Kim, D. K., Zhang, Y., Voit, W., Rao, K. V., & Muhammed, M. (2001). Synthesis and characterization of surfactant-coated superparamagnetic monodispersed iron oxide nanoparticles. *Journal of Magnetism and Magnetic Materials*, *225*(1–2), 30–36. https://doi.org/10.1016/S0304-8853(00)01224-5

LIM, K. O. (1996). CHARCOAL AND GLUCOSE/ETHANOL PRODUCTION FROM OIL PALM AND COCOA PLANTATION WASTES. In *Biomass for Energy and the Environment* (pp. 1516–1521). Elsevier. https://doi.org/10.1016/b978-0-08-042849-9.50012-4

Lou, H., Zhang, Y., Xiang, Q., Xu, J., Li, H., Xu, P., & Li, X. (2012). The real-time detection of trace-level Hg 2+ in water by QCM loaded with thiol-functionalized SBA-15. *Sensors and Actuators, B: Chemical*, *166–167*, 246–252. https://doi.org/10.1016/j.snb.2012.02.053

Luo, X., & Zhang, L. (2009). High effective adsorption of organic dyes on magnetic cellulose beads entrapping activated carbon. *Journal of Hazardous Materials*, *171*(1–3), 340–347. https://doi.org/10.1016/j.jhazmat.2009.06.009

Manocha, S., Manocha, L. M., Joshi, P., Patel, B., Dangi, G., & Verma, N. (2013). Activated carbon from biomass. *AIP Conference Proceedings*, *1538*(1), 120–123. https://doi.org/10.1063/1.4810041

Marsh, H., & Rodríguez-Reinoso, F. (2006). Production and Reference Material. In *Activated Carbon* (pp. 454–508). Elsevier. https://doi.org/10.1016/b978-008044463-5/50023-6

Menéndez-Díaza, J. A., & Martín-Gullónb, and I. (2006). *Types of carbon adsorbents and their production* (Vol. 2006).

Mopoung, S., Moonsri, P., Palas, W., & Khumpai, S. (2015). Characterization and Properties of Activated Carbon Prepared from Tamarind Seeds by KOH Activation for Fe(III) Adsorption from Aqueous Solution. *Scientific World Journal*, *2015*. https://doi.org/10.1155/2015/415961

Mudakavi, J. R., & Puttanna, K. (2016). Decontamination of Chromium Containing Ground Water by Adsorption Using Chemically Modified Activated Carbon Fabric. *Undefined*.

Narzari, R., & Bordoloi, N. (2015). *Biochar - Overview on its Production, Properties and Benefits.pdf* (p. 22). https://doi.org/10.13140/RG.2.1.3966.2560

Osman, Ü., & Yüksel, B. (2018). The effect of carbonization temperature, carbonization time and impregnation ratio on the properties of activated carbon produced from Arundo donax. *Microporous and Mesoporous Materials*, *268*, 225–234. https://doi.org/10.1016/J.MICROMESO.2018.04.037

Pentassuglia, S., Agostino, V., & Tommasi, T. (2018). EAB-electroactive biofilm: A biotechnological resource. In *Encyclopedia of Interfacial Chemistry: Surface Science and Electrochemistry* (pp. 110–123). Elsevier. https://doi.org/10.1016/B978-0-12-409547-2.13461-4

Pongener, C., Kibami, D., Goswamee, R., & Health, S. (2015). *Synthesis and Characterization of Activated Carbon from the Biowaste of the Plant Manihot Esculenta Synthesis and Characterization of Activated Carbon from the Biowaste of the Plant Manihot Esculenta*. *January*. https://doi.org/10.7598/cst2015.958

Rajamani, R., Vinoth Kumar, B., Sujith, A., & Karthick, E. (2018). Activated carbon production from waste biomass. *International Journal of Engineering and*

Technology(UAE), *7*(3.34 Special Issue 34), 345–348. https://doi.org/10.14419/ijet.v7i3.34.19222

Robinson, T., McMullan, G., Marchant, R., & Nigam, P. (2001). Remediation of dyes in textile effluent: A critical review on current treatment technologies with a proposed alternative. *Bioresource Technology*, *77*(3), 247–255. https://doi.org/10.1016/S0960-8524(00)00080-8

Rumi Narzari1, N. B. (2015). Chapter 2- Biochar: An Overview on its Production, Properties and Potential Benefits. In *Biology, Biotechnology and Sustainable Development*. https://doi.org/10.13140/RG.2.1.3966.2560

Safarik, I., Horska, K., Pospiskova, K., & Safarikova, M. (2012). Special Section on Open Door Initiative (ODI)-2 nd edition Magnetically Responsive Activated Carbons for Bio-and Environmental Applications. *International Review of Chemical Engineering (I.RE.CH.E.)*, *4*(3), 346–352.

Samarghandi, M. R., Zarrabi, M., Noori Sepehr, M., Amrane, A., Safari, G. H., & Bashiri, S. (2012). *Application of acidic treated pumice as an adsorbent for the removal of azo dye from aqueous solutions: kinetic, equilibrium and thermodynamic studies* (Vol. 9). https://doi.org/10.1186/1735-2746-9-9

Saputra, E., Trujillo Hernandez, J. S., Muriel, A., Saputra, R., Nugraha, M. W., Irianty, R. S., & Utama, P. S. (2018). *Removal of Methylene Blue from aqueous solution using spent bleaching earth Related content Preparation of Fe 3 O 4 Nanoparticles and Removal of Methylene Blue through Adsorption Removal of Methylene Blue from aqueous solution using spent bleaching earth*. 1–4. https://doi.org/10.1088/1757-899X/345/1/012008

Scott Peterson, J. (2021). *Plant Guide KENTUCKY COFFEETREE Gymnocladus dioicus (L.) K. Koch Plant Symbol = GYDI*. http://npdc.usda.gov

Siemieniewska, K. S. W. S. D. H. E. R. A. W. H. L. M. R. A. P. J. R. T. (1985). *INTERNATIONAL UNION OF PURE AND APPLIED CHEMISTRY PHYSICAL CHEMISTRY DIVISION COMMISSION ON COLLOID AND SURFACE CHEMISTRY INCLUDING CATALYSIS* REPORTING PHYSISORPTION DATA FOR GAS/SOLID SYSTEMS with Special Reference to the Determination of Surface Area a*.

Sudaryanto, Y., Hartono, S. B., Irawaty, W., Hindarso, H., & Ismadji, S. (2006). High surface area activated carbon prepared from cassava peel by chemical activation. *Bioresource Technology*, *97*(5), 734–739. https://doi.org/10.1016/j.biortech.2005.04.029

Sulyman, M., Namiesnik, J., & Gierak, A. (2017). *Low-cost Adsorbents Derived from Agricultural By-products / Wastes for Enhancing Contaminant Uptakes from Wastewater : A Review*. *26*(2), 479–510. https://doi.org/10.15244/pjoes/66769

Takahisa Omata, K. O. and S. O.-Y.-M. (2003). *Photodegradation of Methylene Blue Aqueous Solution Sensitized by Pyrochlore-Related -CeZrO 4 Oxide Powder*. *44*(8), 1620–1623.

Tehrani-Bagha, A. R., & Balchi, T. (2018). Catalytic Wet Peroxide Oxidation. In *Advanced Oxidation Processes for Wastewater Treatment: Emerging Green Chemical Technology* (pp. 375–402). Elsevier Inc. https://doi.org/10.1016/B978-0-12-810499-6.00012-7

Tripathi, N. (2013). Cationic and anionic dye adsorption by agricultural solid wastes: A comprehensive review by: *IOSR Journal of Applied Chemistr*, *5*(3), 91–108. https://doi.org/10.9790/5736-5391108

Valkaj, K., Wittine, O., Margeta, K., Granato, T., Katović, A., & Zrnčević, S. (2011). Phenol oxidation with hydrogen peroxide using Cu/ZSM5 and Cu/Y5 catalysts.

Polish Journal of Chemical Technology, *13*(3), 28–36. https://doi.org/10.2478/v10026-011-0033-6

Vannatta, A. R. (2009). *Ecological Importance of Native Americans Culture to the Kentucky Coffee Tree (Gymnocladus dioicus)*.

Vithanage, M., Mayakaduwa, S. S., Herath, I., Ok, Y. S., & Mohan, D. (2016). Kinetics, thermodynamics and mechanistic studies of carbofuran removal using biochars from tea waste and rice husks. *Chemosphere*, *150*, 781–789. https://doi.org/10.1016/j.chemosphere.2015.11.002

Wang, H., & Chu, P. K. (2013). Surface Characterization of Biomaterials. In *Characterization of Biomaterials* (pp. 105–174). Elsevier Inc. https://doi.org/10.1016/B978-0-12-415800-9.00004-8

Zaya, D. N., & Howe, H. F. (2009). The anomalous Kentucky coffeetree: Megafaunal fruit sinking to extinction? In *Oecologia* (Vol. 161, Issue 2, pp. 221–226). https://doi.org/10.1007/s00442-009-1372-3

Zelmanov, G., & Semiat, R. (2014). Phosphate removal from aqueous solution by an adsorption ultrafiltration system. *Separation and Purification Technology*, *132*, 487–495. https://doi.org/10.1016/j.seppur.2014.06.008

Zhang, X. H., & Li, Q. W. (2017). Carbon fiber spinning. In *Activated Carbon Fiber and Textiles* (pp. 39–60). Elsevier Inc. https://doi.org/10.1016/B978-0-08-100660-3.00003-1

Zheng, Z. (2020). *Magnetic Activated Carbon Production from Lignin and Ferrous Salts Process Modification for Enhanced Phosphate Adsorption from Aqueous Solutions*.

Zubrik, A., Matik, M., Hredzák, S., Lovás, M., Danková, Z., Kováčová, M., & Briančin, J. (2017). Preparation of chemically activated carbon from waste biomass by single-stage and two-stage pyrolysis. *Journal of Cleaner Production*, *143*(November 2017), 643–653. https://doi.org/10.1016/j.jclepro.2016.12.061